Summer 2023

Morphological and Genetic Analysis of the Root System in Two American Grapevines (Vitis Species)

Parinaz Mohtasebi
Missouri State University, pm27s@MissouriState.edu

MORPHOLOGICAL AND GENETIC ANALYSIS OF THE ROOT SYSTEM IN TWO

AMERICAN GRAPEVINES (*VITIS* SPECIES)

A Master's Thesis

Presented to

The Graduate College of

Missouri State University

In Partial Fulfillment

Of the Requirements for the Degree

Master of Science, Biology

By

Parinaz Mohtasebi

August 2023

MORPHOLOGICAL AND GENETIC ANALYSIS OF THE ROOT SYSTEM IN TWO AMERICAN GRAPEVINES (*VITIS* SPECIES)

Biology

Missouri State University, August 2023

Master of Science

Parinaz Mohtasebi

ABSTRACT

The North American grapes species *Vitis rupestris* Scheele and *Vitis riparia* Michx have been the pillars of rootstock breeding for many decades. Though a large body of viticultural knowledge has been accumulated on their impact on grafted scions, the genetic basis of their root system architecture (RSA) has received limited scientific attention. In this study, I generated and analyzed adventitious root systems from dormant cuttings of 22 *V. riparia* and 19 *V. rupestris* accessions, as well as 162 interspecific F1 hybrid progeny from a cross between *V. rupestris* (♀) and *V. riparia* (♂). I photographed the roots and then extracted 23 traits of the RSA from 2-D images using the software RhizoVision Explorer. Principal component analysis (PCA) of seven uncorrelated root traits of the *V. riparia* and *V. rupestris* accessions showed that PC1 explained 57% of the phenotypic variance and arranged the two species into partially overlapping but clearly separate clusters. T-test results demonstrated greater mean for width ($p = 0.00005$), depth ($p = 0.002$), perimeter ($p = 0.002$), lower root area ($p = 0.005$), number of roots ($p = 0.0001$), and total root length ($p = 0.002$) in *V. riparia*, indicating that the overall size of the root system in this species tends to be greater than that in *V. rupestris*. Using a genotype-by-sequencing (GBS) marker-based integrated linkage map and a *V. rupestris* X *V. riparia* F1 progeny, I performed quantitative trait locus (QTL) analysis on 23 root traits. All significant loci were mapped to chromosome 10. A maternal QTL, which mapped to marker S10_4125692 at 21.1 cM, influenced several traits at $p<0.05$, including the maximum width, depth, perimeter, lower root area, and the number of roots of the root system, explaining 12.4-16% of the total phenotypic variance. Using PC-derived scores for 7 high-heritability traits as overall RSA phenotype, a QTL was identified which also mapped to the marker S10_4125692, explaining 13.7% of the variance at $p<0.02$. The novel root QTL identified in this study provides grape breeders with markers for manipulating the size of the root system in new rootstock cultivars.

KEYWORDS: root system architecture, root traits, 2-D images, *Vitis rupestris, Vitis riparia,* rootstock, QTL, linkage map, F1 hybrid progeny

MORPHOLOGICAL AND GENETIC ANALYSIS OF THE ROOT SYSTEM IN TWO

AMERICAN GRAPEVINES (*VITIS* SPECIES)

By

Parinaz Mohtasebi

A Master's Thesis
Submitted to the Graduate College
Of Missouri State University
In Partial Fulfillment of the Requirements
For the Degree of Master of Science, Biology

August 2023

Approved:

Laszlo G. Kovacs, Ph.D., Thesis Committee Chair

Debra S. Finn, Ph.D., Committee Member

Sean P. Maher, Ph.D., Committee Member

Julie J. Masterson, Ph.D., Dean of the Graduate College

In the interest of academic freedom and the principle of free speech, approval of this thesis indicates the format is acceptable and meets the academic criteria for the discipline as determined by the faculty that constitute the thesis committee. The content and views expressed in this thesis are those of the student-scholar and are not endorsed by Missouri State University, its Graduate college, or its employees.

ACKNOWLEDGEMENTS

I dedicate this thesis to my family and friends.

TABLE OF CONTENTS

LIST OF TABLES

LIST OF FIGURES

OVERVIEW

Grafting of woody plants onto rootstock has been performed for more than two millennia. It provides root functions that facilitate higher yields and greater resilience to biotic and abiotic factors [1]. The wild North American grapevine species *Vitis rupestris* Scheele and *Vitis riparia* Michx were selected as grafting rootstocks, first for their resistance to the insect pest phylloxera and high capacity for rooting, subsequently, for to their tolerance to unfavorable abiotic conditions. During the past century and a half, they have become important genetic resources for grape breeding programs [2]. The two *Vitis* species are adapted to different environmental and soil conditions, which is manifested in the architecture and size of their root system [3]. As root system architecture is a critical determinant of water and nutrient foraging ability [4], knowing the difference in particular root features of these two species are of important economic importance. In chapter 1, I generated adventitious roots of the *V. rupestris* and *V. riparia* accessions in controlled condition and comparatively characterized their root system. Adventitious roots are the plant roots that arise from non-root tissues; in this study, the dormant cuttings were used to form the roots.

The shape of the root system of a given plant is controlled by the interactions between genetic and environmental factors [5]. Considering the commercial importance of grapevine and the universal use of rootstocks in vineyards, understanding the genetic underpinnings of grape root system architecture would facilitate the development rootstock cultivars that are well adapted to their environment. In Chapter 2, I undertook genetic mapping to understand the genetic basis of the root system in *V. rupestris* and *V. riparia*. I performed mapping in an F1 progeny generated from an interspecific cross between accessions of these two species and

utilized a single nucleotide polymorphism-based integrated linkage map that was constructed previously [6]. The root trait-linked genetic markers identified in this work can be utilized by breeders to develop rootstocks that better meet climate change-induced challenges of the grape industry.

CHAPTER 1: COMPARATIVE ANALYSIS OF THE ROOT SYSTEM ARCHITECTURE OF *VITIS RUPESTRIS* AND *VITIS RIPARIA*

Introduction

Roots are essential plant organs for water and mineral nutrient acquisition, hormone synthesis, and storage of carbohydrate reserves [1]. In most species, roots anchor the plant to the soil, and in certain lianas specialized aerial roots anchor stems to other plants [2]. Roots absorb large amount of water, most of which moves up to the leaves where it exits through stomata in the form of vapor. This process, termed evapotranspiration, creates a water potential, the negative pressure through which plants draw water from their roots to their other organs to create turgor and to provide reducing power for carbon fixation [3]. Through these functions, the root system plays a pivotal role in the maintenance of both the physiological homeostasis and the structural integrity of the plant [3,4]. In addition, the root system also plays a role in the acclimation of the plant to its environment. The spatial configuration of plant roots, termed "root system architecture" (RSA), can represent a specific adaptive response to the soil environment [5]. The spatial arrangement of roots enables a plant to perform root functions efficiently under the conditions of the climatic and edaphic niche of the species.

RSA is a complex phenotype that emerges from such traits as the number, length, thickness, branching angle, and density of roots [6]. As other organs of the plant, the root system has remarkable plasticity, which is manifested in the response of the RSA to the physical and chemical conditions of the soil [5]. In response to low nitrogen level, for example, the root system forms fewer axial roots and steeper root angles in crown roots in maize, and increased length of lateral roots and decreased root length near the soil surface in *Arabidopsis*. These traits

collectively lead to the exploration of deeper soil layers with higher nitrogen levels [7-9]. In response to low phosphate availability, root length and density increase, root surface area expands in rice, and root hairs become more plentiful in *Arabidopsis* and wheat [10-12]. When roots are exposed to drought stress, the branching angles of pearl millet roots decrease to have access to the deeper layers of the soil where water is more abundant [13]. Lack of root hairs is an appropriate feature for growing in rocky soils with small fissures; the Whiteleaf Manzanita increases the thickness and density of its roots in rocky soils [14].

Grapevine (*Vitis* species) is considered the world's most economically important berry crop which produced 84.79 million metric tons of fruit on 7.31 million hectares in 2021 [15]. Grapes are consumed as wine, juice, fresh fruit, raisins, and jelly [16]. Although cultivated grapevine (*Vitis vinifera* L.) was originally domesticated in the area between the Black Sea and the Caspian Sea and first cultivated around Mediterranean Basin, today it is grown in an extensive area well beyond its native climate zone on both the northern and southern hemispheres [17-19]. The geographic expansion of viticulture was greatly facilitated by grafting and growing grapevines on rootstocks, which were primarily derived from North American *Vitis* species. Two of these species, *V. rupestris* and *V. riparia*, have played a pivotal role in providing the genetic basis for rootstock cultivars [19].

Vitis rupestris and *V. riparia*, are highly polymorphic, heterozygous at most of their genetic loci [20], and their natural populations represent a vast genetic diversity. Collectively, they are adapted to diverse environments and evolved to be resilient to a variety of biotic and abiotic stresses, such as drought, soil salinity, and infestation by nematodes and insect pests [19]. *Vitis rupestris* and *V. riparia* are different eco-species which adapted to specific environmental conditions and have distinct geographic distribution [21]. *Vitis rupestris*, known as rock or sand

4

grape, has a shrub-like growth habit with shoots that lie along the surface of nutrient-poor rocky or sandy gravel bars. It grows in small sporadic populations along streams across an expansive geographic area. *Vitis riparia*, known as riverbank grape, lives in well-drained soils alongside rivers and grows into lianas of high-climbing habit, forming their leaves above the canopies of trees. It grows in large populations over a wide geographic area which largely overlaps the range of *V. rupestris*, but its range extends farther north than that of *V. rupestris* [21] (Figures 1A and B). It has been proposed that the shape and spatial distribution of the root system of these two species, and that their RSA is responsible to a large extent for the differential performance of scions grafted on them. Most data supporting this contention, however, were generated under largely uncontrolled environmental conditions and using only a few individuals representing the species or their hybrids [22]. It is not surprising, therefore, that a recent review of the literature found that grape RSA data are inconclusive [22]. The primary reason for this is three-fold: first, grape root systems are large and hard to access; second, they respond to their soil environment with great plasticity; and third, RSA is a complex phenotype, the accurate description of which is challenging.

Considering the commercial importance of *V. riparia* and *V. rupestris* as rootstock genetic resources, a more precise analysis of their root system is warranted. Therefore, I generated adventitious roots of the two species in controlled condition to characterize their root system through performing a comparative statistical analysis for their root traits.

Methods

Study Design and Root System Generation. Dormant one year-old cuttings from a panel of 24 different genotypes of *Vitis riparia* Michx and 25 genotypes of *V. rupestris* Scheele

5

were obtained from the USDA Grape Germplasm Collection in Geneva, New York. Cuttings of an additional genotype of *V. rupestris* were collected from the Darr Agricultural Center, Springfield, Missouri in December 2021 and January 2022. The cuttings were stored at 4°C for 12 to 15 weeks in moist sawdust to allow them to meet their chilling requirements. For each genotype, 5 cuttings were used as replicates for rooting in the greenhouse, Temple Hall, Missouri State University during May and June of 2022. Rooting was performed at an average temperature of 86ºF and 80% relative humidity [23]. Immediately before rooting, the cuttings were allowed to absorb water by placing them in a beaker filled with water for 24 hours at room temperature. Following rehydration, the cuttings were resected to leave a fresh cut 2 cm below the lowest bud. The remaining two-node stem segments were then weighed and inserted into 17×13 cm plastic pots filled with moist perlite in such a way that the cut surface at the basal end of the stem was positioned 4 cm below the surface of the perlite medium. The pots containing planted stems were placed in a 6 cm deep tray filled with water to maintain a water table 11 cm below the surface of the perlite medium. This positioned the basal end of the stem 7 cm above the water table. The trays were filled with tap water through a water hose and the cuttings were irrigated daily for 5 weeks before photographing the root system [23].

Root System Photographing and RSA Data Extraction. Five weeks post-planting, I removed the rooted vines from perlite and selected three rooted cuttings with the most robust adventitious root system for photographing. I didn't include in my analysis genotypes that had fewer than 3 rooted replicates. Overall, I used 22 genotypes of *V. riparia* and 19 genotypes of *V. rupestris* for analysis. To remove all the perlite attached to the root system, cuttings were carefully washed under running tap water. The cleaned roots were drained by gently tapping them with soft tissue paper. For photographing, a 60 × 60 × 86 cm steel box was constructed

with an LED panel light opposite the open end where a monochromatic-vision camera was affixed 71 cm away from the roots system. I hung the root system by the stem at the top of the box using a retaining clip and captured several two-dimensional greyscale images from all replicates of each genotype from different perspectives. Then, I selected the image in which the root system filled most of the image frame for each replicate. I controlled the camera through the Pylon Camera Software Suite 7.2.0 and saved images in "bmp" file format for analysis (Figures 1C and D).

I carried out the analysis of the root images with the open-source software "RhizoVision Explorer" [24]. This software is a novel 2-D image analysis tool that was designed to provide a reliable quantification of the RSA of plants by extracting and recording 23 traits of the root system phenotype, plus providing computational time which is the time taken to analyze the root image. The root traits were extracted and analyzed from each root image, and the data were stored in CSV format. I provide the description of the traits based on Seethepalli et al [24] with additional explanation in Table 1. The traits characterize the root system in terms of the maximum and median number of roots, total root length, maximum width, depth, width to depth ratio, network area, convex area, solidity, lower root area, average diameter, median diameter, maximum diameter, perimeter, total root volume, surface area, holes, average root orientation, shallow angle frequency, medium angle frequency, steep angle frequency, and projected area. The software also provided the root length, the volume, the surface area, and the projected area of the root system in three different ranges of diameter of the roots. The software provided all measurements in pixels. After taking a photograph of an object of known size (a US one-cent coin), I calculated that the length of 1 pixel corresponded to 0.152 mm, and converted all length, area, and volume measurements to units of the metric system.

Statistical Analysis. First, I calculated the average of three replicates for each genotype, and the means and standard deviations of each root trait for each species using Microsoft Excel software; then, I examined the normality of data distribution by considering the histogram for each trait. For data with non-normal frequency distribution, I used log-transformation to convert the data to approximate normal distributions (Appendix A-1). A previous study has shown that many of the grape root traits I measured are not heritable, but mostly under the control of the environment [23], confirming the high-level phenotypic plasticity of the root system [22]. I reasoned those traits that are not under genetic control cannot be consistent features of genotypes and, therefore, I focused my analysis on those traits that were shown to be influenced by the grape genome. These were median and maximum number of roots, total root length, maximum width, network area, convex area, average diameter, median diameter, perimeter, and surface area [23]. I performed a statistical comparison of means between the two species by applying parametric two-sample Student's *t*-test for log-transformed data, and non-parametric Mann-Whitney U-test for non-transformed data. I created bar graphs via GraphPad Prism 6.0 to compare the means between two species for some root traits. Two measurements were considered different if their values differed at $p<0.05$. I performed correlation analysis among RSA traits using Pearson's correlation test and a heatmap was generated for each species separately to examine positive and negative correlations between root traits. RSA is a complex phenotype, a composite of various components, and each component is defined as a root trait. I characterized RSA by measuring and analyzing the different root traits. Many of these traits are expected to highly correlate with one-another in both *V. rupestris* and *V, riparia*. For example, a greater root length is expected to be coupled with a higher total surface area and volume. Additionally, I applied regression analysis to examine the effect size of certain root traits that

were expected to have effect on particular traits (Appendix A-2). To reduce the dimensionality of the RSA phenotype data, I performed a principal component analysis (PCA) through the "prcomp" function in R. First, I conducted a PCA with all root traits regardless of whether any of the traits is correlated with one-another (Appendix A-3). PCA plots containing ellipses were generated using "ellipse" package in which the ellipses represent the difference between two species in terms of their distribution around first two principal components (PCs) with 95% confidence interval. Then, I removed intercorrelated traits (r >0.8 and r <-0.8), which resulted in 7 traits that explained most variations in two species. All statistical analyses were performed using R scripts, which are shown in the Appendix B.

Results

  Statistical Comparison of RSA Traits between Two Species. I observed several of the traits to be significantly different between *V. rupestris* and *V. riparia* applying both U-tests and *t*-tests (Table 2). For many traits, including maximum number of roots, median number of roots, total root length, depth, maximum width, network area, convex area, lower root area, perimeter, surface area, holes, volume in small and medium diameters, in addition to computation time and the three different diameter ranges for projected area, root length, and surface area, the mean value was greater in *V. riparia* compared to *V. rupestris* (*p*<0.05) (Table 2 and Figure 2). On the other hand, solidity, average diameter, median diameter, and steep angle frequency had greater means in *V. rupestris* than in *V. riparia* applying both statistical tests (Table 2). There was no significant difference between two species regarding maximum diameter, volume in large diameter range, shallow angle frequency, medium angle frequency, and width-to-depth ratio. Furthermore, the mass of *V. riparia* and *V. rupestris* dormant stems used to generate the

9

adventitious roots were statistically indistinguishable from one another (Figure 3). The binomial test for the number of all root traits and the number of traits that had greater mean in *V. riparia* was significant (*p*=0.04); however, by considering the uncorrelated traits in *V. riparia* including maximum number of roots, average diameter, medium angle frequency, average root orientation, and depth that had greater mean in *V. riparia*, the binomial test was not significant (*p*= 0.6).

Correlation Analysis and Effect Size Examination in Two Species. Pearson correlation coefficient (r) between root length and surface area, and root length and volume were above 0.7 in both species (Figure 4). Average root orientation (the angle of a root from the horizontal line) and the frequency of steep angles are both the characteristic of steep-striking roots; as expected, the r value between them was 0.9. Consequently, average root orientation is negatively correlated with frequency of shallow angles in both *V. rupestris* (r = -0.9, *p* =0.0000001) and *V. riparia* (r = -0.8, *p* = 0.00000003).

In general, traits that were associated with the overall size of the root system had the tendency to have positive pairwise correlations (r > 0.7). This included volume, surface area, root length as a whole and in three diameter ranges, holes, perimeter, lower root area, convex area, network area, depth, maximum width, median and maximum number of roots. The lower root area (the 2-D area projected below the longest latitude of the system) was highly correlated with all size-associated traits (r> 0.7) in both species (Figure 4). This is supported by the observation that depth of the root system strongly correlated with lower root area, convex area, and network area in both species (0.85<r< 0.95). Traits that did not correlate with the size of the root system in either species were root orientation and angle frequency. The frequency of shallow, medium, or steep angles did not correlate with size (Figure 4). Unexpectedly, neither root orientation, nor the frequency of steep angles correlated well with depth of the root system in either parent.

Nonetheless, regression analysis for the effect of steep root angle on the depth was significant in *V. riparia* since the F-test value was much greater than 1 in this species (F = 24.09, R^2= 0.54, DF=20), but not in *V. rupestris* (F = 0.01, R^2= 0.0009, DF=17) (Appendix A-2). Although there was no correlation between depth and steep angle frequency in either species, the steeper angles lead to deeper root in *V. riparia*. Maximum root diameter also had no correlation with overall size or the depth of the root system in either species, but it was highly correlated with volume in *V. rupestris* (r= 0.74, *p* =0.0002) (Figure 4A). In *V. riparia*, the average root diameter had a strong negative correlation with size-associated traits root length, projected area, surface area, and volume in medium root diameter range (r <-0.8) (Figure 4B).

      Exploratory Data Analysis. Following the performance of PCA for all traits, I found that the first two principal components (PCs) captured 84.9% of the variation, with PC1 and PC2 explaining 72.5% and 12.4% of the variation, respectively (Appendix A-3). PC1 correlated well with volume, surface area, projected area, root length, maximum diameter, perimeter, convex area, lower root area, number of roots, holes, maximum width, network area, and the volume and surface area of entire root system, while PC2 correlated well with shallow angle frequency, medium angle frequency, average root orientation, steep angle frequency, width-to–depth ratio, median diameter, average diameter, and solidity. The ellipses with 95 % confidence interval placed the two species into non-overlapping clusters that clearly demonstrated the difference in the root system of the two species. The highly correlated size-associated traits in PC1 were directed toward the cluster of *V. riparia*. Following the removal of the interrelated root traits with high negative and positive correlations, the dimensions of the PCA plot decreased to seven root traits which represented the cumulative variation of 84.7% in the first two PCs (Figure 5). Considering the loadings in the PCA plot and the 95% confidence interval shown by ellipses, the

11

volume, maximum number of roots, convex area, and depth heavily loaded on PC1, and were

directed toward the cluster of *V. riparia* in which the mean values for those traits were greater

compared to *V. rupestris*; these four traits indicated the same directions in the PC1 which

explains 57.2% of the variation. The average diameter, however, was more toward the *V.

rupestris* in PC1. The traits that heavily loaded on PC2 were average root orientation and

medium angle frequency.

Discussion

The results of statistical comparison clearly indicated the difference in the overall root

system between *V. rupestris* and *V. riparia*, and the greater size of the root system in *V. riparia*.

Although the geographic range of the two species overlap in some areas, the findings of this

chapter indicate that the two species may have evolved specific features in their root system

based on specific ecological condition in their natural habitat. The literature, however, is replete

with information on their different root adaptations in response to their soil environment despite

their mutual geographic range. A recent analysis of the climate attributes of thirteen North

American *Vitis* species demonstrated that the climate niche and the geographic range of *V.

rupestris* is almost entirely nested within those of *V. riparia* [25] (Figures 1A and B). *Vitis

riparia* and *V. rupestris* are also closely related phylogenetically [26], suggesting that their

shared geographic distribution is the consequence of having had a shared common ancestor

which occupied the same climatic niche. This phenomenon, termed evolutionary conservatism,

has been observed for several North American *Vitis* clades by Callen et al [25]. Closely related

species that share the same climatic niche and geographic range often adapt to different fine-

scale ecological conditions and evolve different morphological features that enable them to

specialize to live in unique habitats. *Vitis riparia* and *V. rupestris* are classic example of such specialization, as they live not only in sympatry, but often grow along the same rivers. *Vitis riparia* grow in the moist, rich soil of the floodplains, whereas *V. rupestris* inhabits rocky riverbanks and gravel bars, and dried-up riverbeds of intermittent rivers [27]. Adaptation to these different niches lead to the evolution of strikingly different morphology: *V. riparia* grows into large lianas that climb on trees and form leaves high in the forest canopy, while *V. rupestris* grows into shrubs directly on the surface of gravel, sand or rocks. Callen et al [25] speculated that adaptation to different soil conditions may have played a major part in the divergence of these two *Vitis* species but did not analyze soil attributes of their habitats. The viticulture literature confirms this adaptation-to-soil hypothesis. As both *V. riparia* and *V. rupestris* are used extensively as rootstock varieties (*V. riparia* 'Gloire de Montpellier' and *V. rupestris* 'St. George'); they have been observed to be best suited for deep moist and dry and rocky vineyard soils, respectively [28]. The root system of these two rootstock varieties has been examined under various conditions. For example, in 1905, Guillon observed shallow and steep emergence angles of *V. riparia* 'Gloire de Montpellier' and *V. rupestris* 'St. George' and concluded that the former developed a spreading root system with obtuse root orientation, while the latter formed a deep-striking root system with acute root orientation [22]. Several subsequent observations on grape root distribution, using glass rhizotrons, hydraulic excavation, and profile wall methods, either confirmed or contradicted this notion. The inconsistent results are likely due to conducting most of these observations in dissimilar vineyard soil, where non-homogeneous mineral distributions, obstacles and penetration barriers impacted the phenotypic plasticity of the roots. Furthermore, experiments and observations were carried out on a handful of grape genotypes with limited number of replications, and analytical methods to adequately characterize the

13

complex phenotype of the grape RSA also were lacking. A comprehensive synthesis of the grape RSA literature by Smart and co-workers [22] found that root distribution data for several rootstock genotypes, among them *V. rupestris* 'St. George' were woefully inconsistent. There has been no experimental analysis of grapevine RSA where environmental conditions were kept constant. In this chapter, however, I addressed this knowledge gap; for the first time, I characterized the RSA of the two species in controlled conditions and I used the average of three replicates for each genotype in data analysis which not only reduced the environmental impact but also the sampling bias to a large degree.

In this study, the frequency of medium and shallow angles was not different between the species. The angle is an important determinant in RSA that leads to the development to a shallow or steep root system, and it has considerable effects on water and nutrients uptake [29]. The differences in root angles in various regions of plant's root system is suggested to decrease the self-competition of roots that can boost the efficiency of soil exploration [30]. In case of water deficiency and drought stress condition in soil, the roots increase their orientation to have access to deep soil where the water is abundant, and steeper root angles may be an appropriate adaptation for the exploration of the deeper soil layers [13]. Surprisingly, the mean values of all size-related traits were greater in *V. riparia* than *V. rupestris*, and these findings were well compatible with the direction of loadings of PC1 for all root traits. While the root depth was significantly greater in *V. riparia*, the frequency of steep angles was more abundant in *V. rupestris*. Narrow angle roots can expand in soil depth, whereas wide angle roots grow in low depth that allow plants to absorb nutrients, such as phosphorus, that are more abundant in the topsoil [31].

In a normal healthy plant, there must be a balance between total surface area of the leaves and tissue exposed to the sun to absorb the energy and generate carbohydrates, in relation to total root surface area exposed to soil environment to absorb mineral and water [2]. In some time periods such as the end of growth season, the root system might be equal or greater than the aboveground shoot system, as in this season the roots might penetrate to high depth and have lateral growth in diameter while the growth at the top is more limited [2]. Since the root system was analyzed 5 weeks after planting, the growth and the surface area of the leaves were similar and considerably great in both species; however, the entire surface area of the root system, in addition to the surface area in small, medium, and large diameter ranges were significantly greater in *V. riparia* than the *V. rupestris*; these findings were not surprising though since *V. riparia* grows into large vines and the overall root system of which is expected to be larger than *V. rupestris*. In both *V. rupestris* and *V. riparia*, the surface area was strongly correlated with number of roots, total root length and the root length in small, medium, and large diameters, network area, convex area, lower root area, perimeter, volume in small and medium diameters, and projected area in small, medium, and large diameters of the root system, all of which have great contribution to the size of the root system. Remarkably, lower root area strongly correlated with all size-associated traits in both species, indicating that grapevine has the tendency to expand its roots in the lower soil layers. The lack of high positive correlation between depth and steep angle frequency was unexpected as it is in disagreement with the generally accepted notion that roots emerging in a steep angle result in a deep-striking root system. However, the regression analysis showed the significant effect of steep angles on the depth of the root system in *V. riparia*. Although *V. riparia* possessed an overall larger root system, its initial mass of the propagule from which it arose was not significantly greater than that of *V. rupestris*. This finding

can lead to a conclusion that, when these species form adventitious roots, *V. riparia* invest more of its resources into root system development than does *V. rupestris*. It is important to emphasize that my experimental conditions have limited our observations to the early stages of root development. Therefore, our results cannot be extrapolated to the RSA of older, well-established vines.

Although plant root system and the role of plant roots in anchorage and absorption have been studied since a century ago, roots are still the plant organs with the least scientific attention due to their underground growth and the complicated functions of the root system for soil exploration [32]. As the role of different angles to reduce roots self-competition has been suggested [2], it is likely that the root system of these two species have the same level of self-competition since there was no significant difference in terms of the frequencies of the shallow and medium angles. In nitrogen deficiency situation [7-9], the two species seem to have the same opportunity to tolerate this nutrient stress, as carrying both steeper roots angles and longer roots could lead to improved function where the nitrogen level is low. Regarding phosphate deficiency conditions [10-12], it is likely that *V. riparia* have a greater chance to survive than *V. rupestris* since possession of longer roots, greater number of roots, and lower frequency of sharp angles would lead to a better exploration of roots to access the small amount of phosphate.

It has been indicated that several plant species, including grapevines, enter into a symbiotic relationship with arbuscular mycorrhizal fungi (AMF) [33]. AMFs are fungal species and are important soil microorganisms that can positively affect the grapevine crops and are beneficial soil microorganisms for *Vitis* species since they can establish symbiotic associations with *Vitis* roots that lead to positive effects on grapevine performance in terms of water use efficiency, nutrient uptake, and success in replanting [34]. AMFs are critical due to providing an

increased interface between roots and soil and improving the plant nutritional state, particularly for phosphate as they are present in the topsoil at the depth of around 30cm, where phosphate is abundant [34]. In areas with seasonally flooded soils, floodwater phosphate concentration can increase up to 3.6 times the initial concentration in a range from 0.032 to 3.70 mg/L [35]. A study reported greater amount of total organic phosphate in the floodplain environment (277.27mg/ kg) compared to the upland areas (113.04mg/ kg) [36]. As *V. riparia* inhabits well-drained soils of floodplain areas, it would be an interesting and worthwhile research endeavor to explore the association of this species with AMF. Also, it would be interesting to look at the AMF relationships with *Vitis* species that live in phosphate-poor soils. Unfortunately, information on the edaphic conditions under which native grapevines grow is scarce. However, because I used perlite without application of fertilizers or mycorrhizal fungi, the effect of these beneficial microorganisms cannot be accurately determined in this study as it was carried out in controlled conditions.

The findings of this chapter would be a steppingstone for the evaluation of the root system of the resulting F1 progeny from a cross between these two species to identify the genomic regions associated with root traits and the inheritance pattern of the root traits. The strict control of environmental conditions, however, comes at the price of limitations; the 5-week rooting period was short, and the root system was studied in early life of the newly propagated plants with small volume of roots. The available space of greenhouse was limited, and only five replicates of each genotype could be planted for rooting; the time of collection and storing of the cuttings were not uniform and some of the cuttings were stored in sawdust for longer time than the others; the temperature could not perfectly be controlled during the entire rooting procedure. In addition, it needs to be mentioned that the sample size for this study was quite small; in this

case, the *p*-values of statistical tests could be due to a random chance and this research needs to be repeated in the future with larger sample size for both species to be increase confidence and reduce uncertainty in results. For instance, the regression analysis for the effect of steep angle frequency on depth was significant in *V. riparia* but was not significant in *V. rupestris.* One important finding in my results was that the size of the root system was considerably greater in *V. riparia,* and that could be clearly demonstrated by comparing the overall root shape in the two-dimensional images captured from the two species. Regarding adaptations of the two species based on their original location, we may need to take into account that the rooting of the two species were carried out in controlled conditions; therefore, the lack of difference for shallow and medium angle frequencies between two species could be due to growing in the same and constant environmental conditions since the angles are highly affected by environmental factors, rather than the genome of the plant.

References

1. Palta JA, Yang J. Crop root system behaviour and yield. Field Crops Res. 2014;165:1–4.

2. Robbins WW, Weier TE, Stocking CR. Botany: an introduction to plant science. 2nd ed. London: Cahpman and Hall; 1957.

3. Tajima R. Importance of individual root traits to understand crop root system in agronomic and environmental contexts. Breed Sci. 2021;71(1):13-9.

4. Smith S, Smet I. Root system architecture: insights from Arabidopsis and cereal crops. Philos Trans R Soc Lond B Biol Sci. 2012;367(1595):1441-52.

5. Hodge A. The plastic plant: root responses to heterogeneous supplies of nutrients. New Phytol. 2004;162 (1):9-24.

6. Khan MA, Gemenet DC, Villordon A. Root system architecture and abiotic stress tolerance: current knowledge in root and tuber crops. Front Plant Sci. 2016;7:1–13.

7. Trachsel S, Kaeppler SM, Brown KM, Lynch JP. Maize root growth angles become steeper under low N conditions. Field Crops Res. 2013;140:18–31.

8. Gruber BD, Giehl RFH, Friedel S, Wiren NV. Plasticity of the Arabidopsis root system under nutrient deficiencies. Plant Physiol. 2013;163:161–79.

9. Zhan A, Lynch JP. Reduced frequency of lateral root branching improves N capture from low-N soils in maize. J Exp Bot. 2015;66:2055–65.

10. Flavel RJ, Guppy CN, Tighe MK, Watt M, Young IM. Quantifying the response of wheat (*Triticum aestivum* L) root system architecture to phosphorus in an Oxisol. Plant Soil. 2014;385:303–10.

11. Kawa D, Julkowska MM, Sommerfeld HM, Horst AT, Haring MA, Testerink C. Phosphate-dependent root system architecture responses to salt stress. Plant Physiol. 2016;172:690–706.

12. Nestler J, Wissuwa M. Superior root hair formation confers root efficiency in some, but not all, rice genotypes upon P deficiency. Front Plant Sci. 2016;7:1935.

13. Passot S, Gnacko F, Moukouanga D, Lucas M, Guyomarc HS, Ortega BM, et al. Characterization of pearl millet root architecture and anatomy reveals three types of lateral roots. Front Plant Sci. 2016;7:11.

14. Zwieniecki MA, Newton M. Roots growing in rock fissures: their morphological adaptation. Springer. 1995;172:181-7.

15. United nations Food and Agriculture Organization. FAOSTAT, United States of America; 2023 [cited 2023 Feb 23]. Available from: https://www.fao.org/statistics/en/.

16. Grassi F, Lorenzis GD. Back to the origins: background and perspectives of grapevine domestication. Int J Mol Sci. 2021;22(9):4518.

17. Londo JP, Johnsonb LM. Variation in the chilling requirement and budburst rate of wild *Vitis* species. Environ Exp Bot. 2013;106:138–47.

18. Hannah L, Roehrdanz PR, Ikegami M, Shepard AV, Shaw MR, Tabor G, et al. Planning for agricultural adaptation to climate change and its consequences for conservation. Proc Natl Acad Sci U S A. 2013;110(33):6907–12.

19. Ollat N, Bordenave L, Tandonnet JP, Boursiquot JM, Marguerit E. Grapevine rootstocks: origins and perspectives. Acta Hortic. 2016;1136:11–22.

20. Liang Z, Duan S, Sheng J, Zhu S, Ni X, Shao J, et al. Whole-genome resequencing of 472 *Vitis* accessions for grapevine diversity and demographic history analyses. Nat Commun. 2019;10:1190.

21. Klein LL, Miller AJ, Ciotir C, Hyma K, Uribe-Convers S, Londo J. High- throughput sequencing data clarify evolutionary relationships among North American *Vitis* species and improve identification in USDA *Vitis* germplasm collections. Am J Botany. 2018;105:215–26.

22. Smart DR, Schwass E, Lakso A, Morano L. Grapevine rooting patterns: a comprehensive analysis and a review. Am J Enol Vitic. 2006;57:89-104.

23. Thapa S. Analysis of root system architecture and QTL identification in grapevines [Master's Thesis]. Springfield, MO: Missouri State University; 2022.

24. Seethepalli A, Dhakal K, Griffiths M, Guo H, Freschet GT, York LM. RhizoVision Explorer: open-source software for root image analysis and measurement standardization. AoB Plants. 2021;13(6):plab056.

25. Callen ST, Klein LL, Miller AJ. Climatic niche characterization of 13 North American *Vitis* species. Am J Enol Vitic. 2016;67:339-49.

26. Zecca G, Abbot JR, Sun WB, Spada A, Sala F, Grassi F. The timing and the mode of evolution of wild grapes (*Vitis*). Mol Phylogenet and Evol. 2012;62:736-47.

27. Pap D, Miller AJ, Londo JP, Kovacs LG. Population structure of *Vitis rupestris*, and important resource for viticulture. Am J Enol Vitic. 2015;66:403-10.

28. Pongracz DP. Rootstocks for Grape-vines. Cape Town: David Philip; 1983.

29. Ge ZY, Rubio G, Lynch JP. The importance of root gravitropism for inter-root competition and phosphorus acquisition efficiency: results from a geometric simulation model. Plant Soil. 2000;218:159–71.

30. Morris EC, Griffiths M, Golebiowska A, Mairhofer S, Burr-Hersey J, Goh T, et al. Shaping 3D root system architecture . Curr Biol. 2017;27(17):R919-30.

31. Miguel MA, Postma JA, Lynch JP. Phene synergism between root hair length and basal root growth angle for phosphorus acquisition. Plant Physiol. 2015;167:1430–9.

32. Hochholdinger F. Untapping root system architecture for crop improvement. J Exp Bot. 2016;67(15):4431–3.

33. Cesaro P, Massa N, Bona E, Novello G, Todeschini V, Boatti L, et al. Native AMF communities in an Italian vineyard at two different phenological stages of *Vitis vinifera.* Front Microbiol. 2021;12:676610.

34. Massa N, Bona E, Novello G, Todeschini V, Boatti L, Mignone F, et al. AMF communities associated to *Vitis vinifera* in an Italian vineyard subjected to integrated pest management at two different phenological stages. Sci Rep. 2020;10:9197.

35. Young EO, Ross DS. Phosphate release from seasonally flooded soils: a laboratory microcosm study. J Environ Qual. 2001;30(1):91-101.

36. Arenberg MR, Liang X, Arai Y. Immobilization of agricultural phosphorus in temperate floodplain soils of Illinois, USA. Biochem. 2020;150: 257-78.

Table 1. RSA traits extracted from 2-D images of root systems by RhizoVision Explorer.

Trait	RhizoVision Analyzer Function
Median number of roots and maximum number of roots	A horizontal line scan is performed on each segmented image and the number of pixel transitions is recorded to calculate the median and the maximum number of roots. These traits provide a measure of how extensive a root system is in terms of the number of individual root strands that compose it.
Number of root tips	The pixels in identified root topology with only one neighboring skeletal pixel. This trait provides the total number of root strands that compose the entire root system.
Total root length	Total Euclidean distance between connected skeletal pixels in the entire root topology in a skeletonized image (root length was also computed and binned based on three specified diameter ranges *).
Depth, maximum width, and width-to-depth ratio	The maximum vertical and horizontal distance the root crown grew at the time of imaging are depth and maximum width, respectively. The ratio of maximum width to depth of the image is noted as the width-to-depth ratio.
Network area, convex area, and solidity	The total number of pixels enclosing roots in a segmented image is noted as the network area. The area of convex hull in which a root can fit is defined as the convex area. The ratio of network area to convex area is defined as solidity.
Average, median, and maximum diameters	The value of transformed distance at each skeletal pixel is the radius at that pixel and is doubled to give the diameter. The average, median and maximum diameters are computed across all these skeleton pixels.
Perimeter, volume, and surface area	Total Euclidean distance between the contour pixels is noted as perimeter. Using the diameter calculated above, the volume is length of the pixel multiplied by the cross-sectional area of the root at that pixel (volume was also computed and binned based on three specified diameter ranges *). The surface area is calculated as the length of the pixel multiplied by the circumference of the cross-section of the root at that pixel (surface area was also computed and binned based on three specified diameter ranges *).
Lower root area	The lower root area is the network area of the segmented image pixels that are located below the location of the medial axis pixel that has the maximum radius.

Table 1. continued

Holes	The background components between roots in a segmented image are noted as holes.
Shallow, medium, steep angle frequencies, and average root orientation	Given the skeletal image, for every pixel in the medial axis, the locations of the medial axis pixels in a 40*40-pixel locality are used to determine the orientation of these pixels in the locality. These orientations are grouped in bins of 0° to 30°, 30° to 60°, and 60° to 90° and their frequencies as steep, medium, and shallow angle frequencies. The average root orientation is the average of these orientations.
Projected area	The projected area on the surface of the image plane at each skeletal pixel. It was computed and binned based on three specified diameter ranges *.

*Range 1 (small roots) refers to dimeter range 0-0.304 mm, range 2 (medium-size roots) to diameter range 0.305-0.760 mm, and range 3 (large roots) refers to diameter greater than 0.760 mm.

Table 2. Propagule mass and RSA traits in *V. rupestris* and *V. riparia*.

Trait	Mean ± SD		P value[†]	
	V. rupestris	*V. riparia*	t-test	U-test
Mass of Propagule	5.42± 2.16	5.91±1.84	0.4	0.2
Median Number of Roots	4.7± 1.47	6.87±2.77	0.003	0.004
Maximum Number of Roots	14.22±4.6	21.27±5.81	0.0001	0.0002
Number of Root Tips	112.98±71.09	225.39±153.53	0.006	0.004
Total root length (mm)	1215.76±799.34	2893.01±1972.57	0.002	0.001
Depth (mm)	83.61±36.37	139.27±66.41	0.002	0.003
Maximum width (mm)	68.3±22.53	109.45±33.71	0.00005	0.00009
Width-to-Depth Ratio	0.92±0.29	0.94±0.37	0.8	1
Network area(mm^2)	1424.25±872.91	2963.49±1999.39	0.005	0.003
Convex area (mm^2)	4402.78±2855.14	11686.54±8097.97	0.001	0.0004
Solidity	0.34±0.66	0.28±0.07	0.004	0.002
Lower root area (mm^2)	1281.88±792.96	2771.72±1882.14	0.005	0.003
Average diameter (mm)	2.6±0.54	2.10±0.44	0.002	0.004
Median diameter (mm)	1.7±0.25	1.44±0.19	0.001	0.004
Maximum diameter (mm)	16.3±3.23	17.12±2.29	0.3	0.2
Perimeter (mm)	1431.75±936.21	3632.76±2578.85	0.002	0.0009
Volume (mm^3)	13587.4±10111.77	18819.43±12822.58	0.07	0.1
Surface area (mm)	9335.08±5814.29	17484.93±11586.41	0.007	0.004
Holes	112.73±87.2	310.91±222.71	0.002	0.0007
Average Root Orientation (deg)	49.3±3.52	47.18±2.69	0.03	0.06
Shallow Angle Frequency	0.26±0.03	0.28±0.03	0.06	0.2

Table 2. continued

Medium Angle Frequency	0.33±0.04	0.35±0.03	0.08	0.06
Steep Angle Frequency	0.4 ±0.07	0.35±0.05	0.02	0.01
Computation time	0.07±0.02	0.13±0.06	0.0007	0.0007
Root. Length. Diameter. Range.1 (mm)	66.88±44.55	181.24±136.06	0.003	0.001
Root. Length. Diameter. Range.2 (mm)	184.58±150.46	536.40±417.30	0.002	0.0006
Root. Length. Diameter. Range.3 (mm)	964.29±600.53	2175.36±1467.53	0.002	0.001
Projected. Area. Diameter. Range.1 (mm^2)	20.12±13.41	54.42±40.99	0.003	0.001
Projected. Area. Diameter. Range.2 (mm^2)	108.32±88.27	314.82±243.17	0.002	0.0006
Projected. Area. Diameter. Range.3 (mm^2)	2841.99±1777.53	5194.05±346211	0.009	0.008
Surface. Area. Diameter. Range.1 (mm^2)	63.22±42.14	171.02±128.81	0.003	0.001
Surface. Area. Diameter. Range.2 (mm^2)	340.35±277.39	989.21±764.08	0.002	0.0006
Surface. Area. Diameter. Range.3 (mm^2)	8931.5±5586.75	16324.69±10881.92	0.009	0.008
Volume. Diameter. Range.1 (mm^3)	4.8±3.2	12.99±9.78	0.003	0.001
Volume. Diameter. Range.2 (mm^3)	51.26±41.75	148.98±114.36	0.002	0.0006
Volume. Diameter. Range.3 (mm^3)	13531.33±10093.84	18657.45±12743.98	0.07	0.1

[†]p-value as calculated with two-sample t-test and Mann-Whitney U-test. Values were considered different at $p<0.05$.
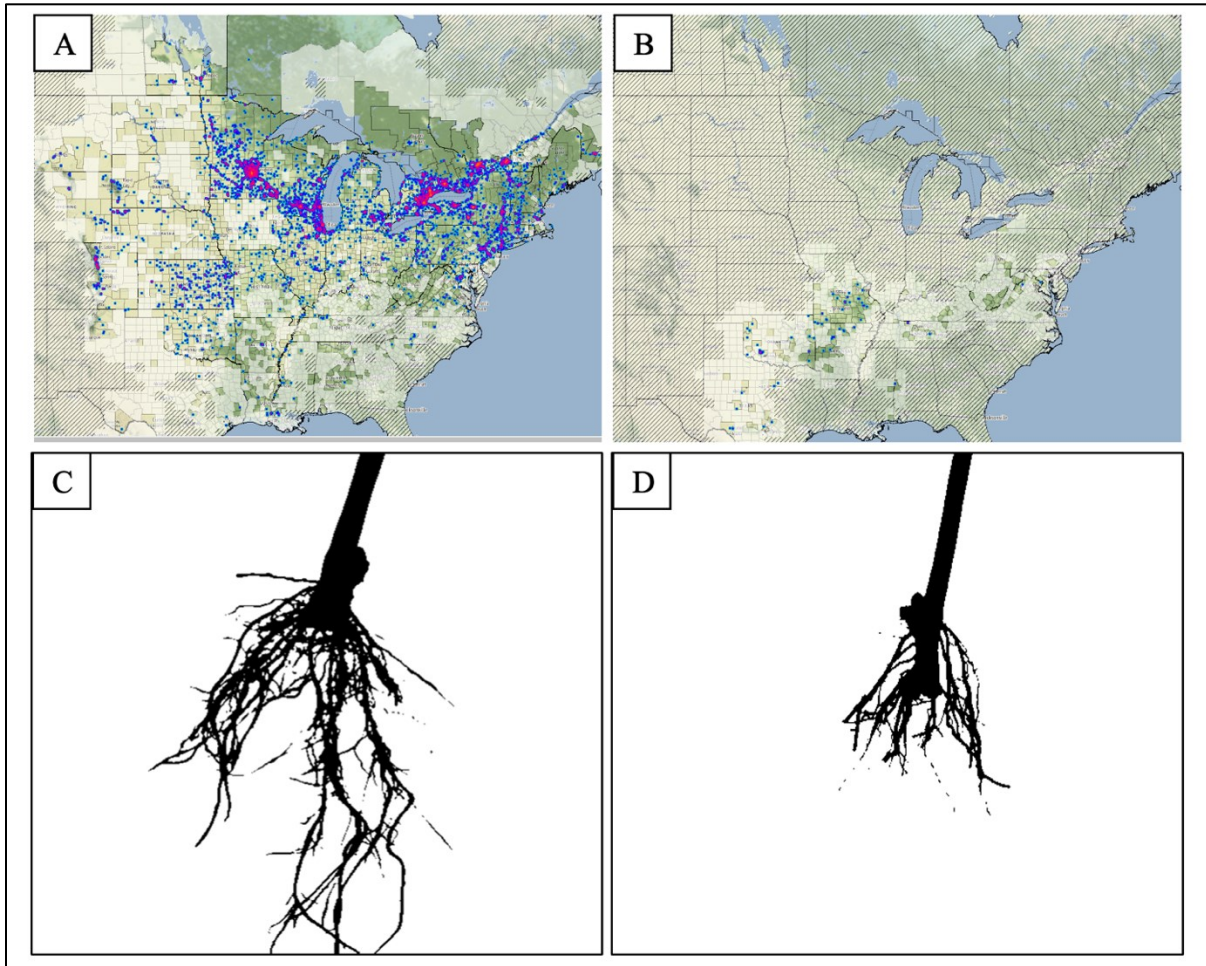
Figure 1. Geographic range and photographic images of root systems of *V. riparia* (A and C) and of *V. rupestris* (B and D). In panels A and B, light blue dots show locations where a specimen of the species has been collected; the intensity of the blue and magenta colors are commensurate with number of specimens collected in the area. Green- and beige-colored areas indicate counties where the species has been documented and expected to occur, respectively. Hatching indicates regions where the species is not expected to occur naturally (maps from www. wildflowersearch.org).
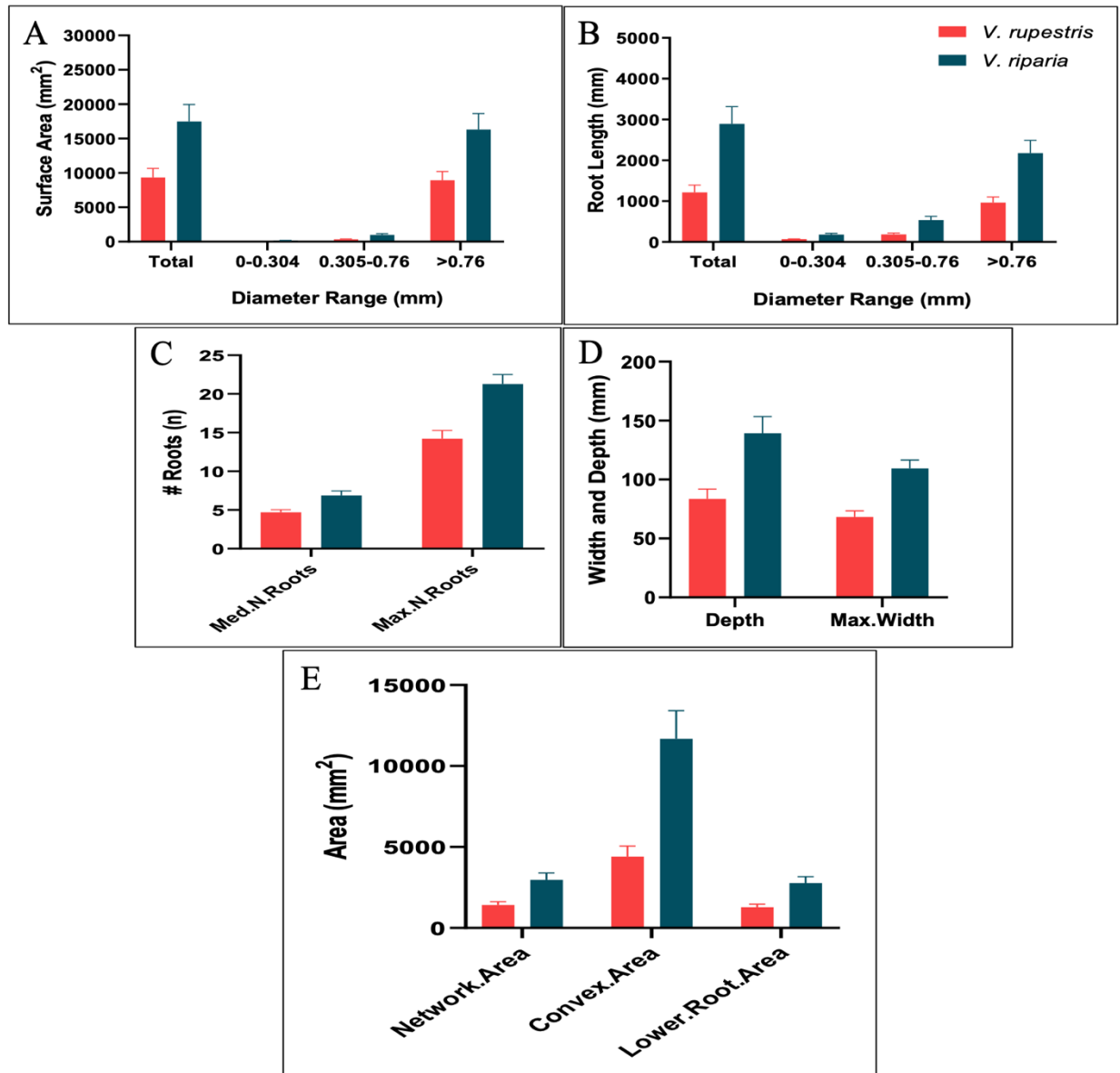
Figure 2. Size-related traits are different in *V. rupestris* and *V. riparia.* (A) Mean of root surface area in three root diameter ranges (range 1= 0-0.304 mm; range 2= 0.305-0.76 mm; range 3>0.76 mm); (B) Mean of total root length, and in three root diameter ranges; (C) Mean of maximum number of roots and median number of roots; (D) Mean of maximum width and depth (E) Mean of network area, convex area, and lower root area. Error bars represent SE. For all traits difference is significant at $p<0.05$.
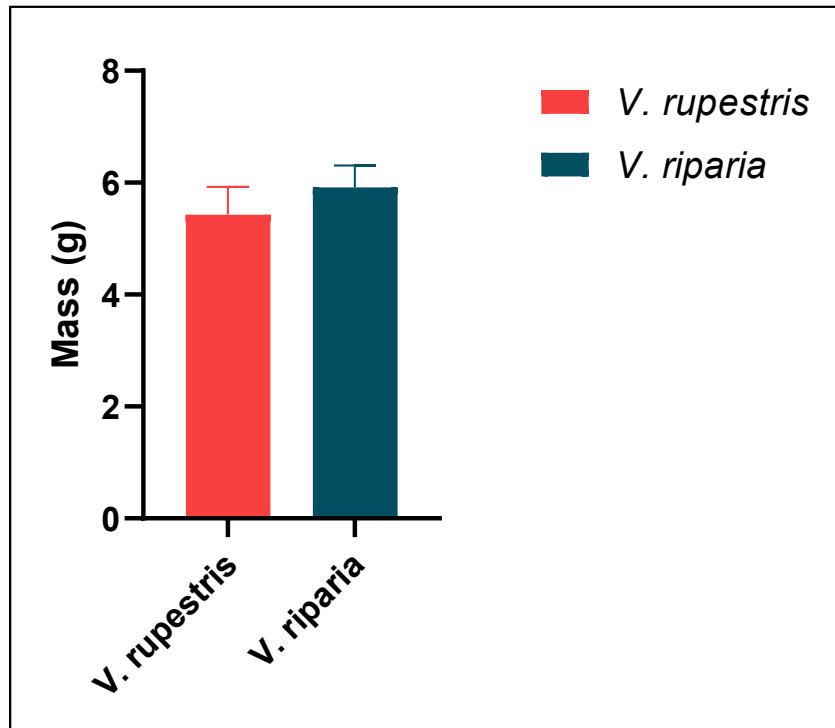
Figure 3. Mean of initial mass of dormant stem propagules in *V. riparia* and *V. rupestris*. Error bars represent SE. The significance level is at $p<0.05$.
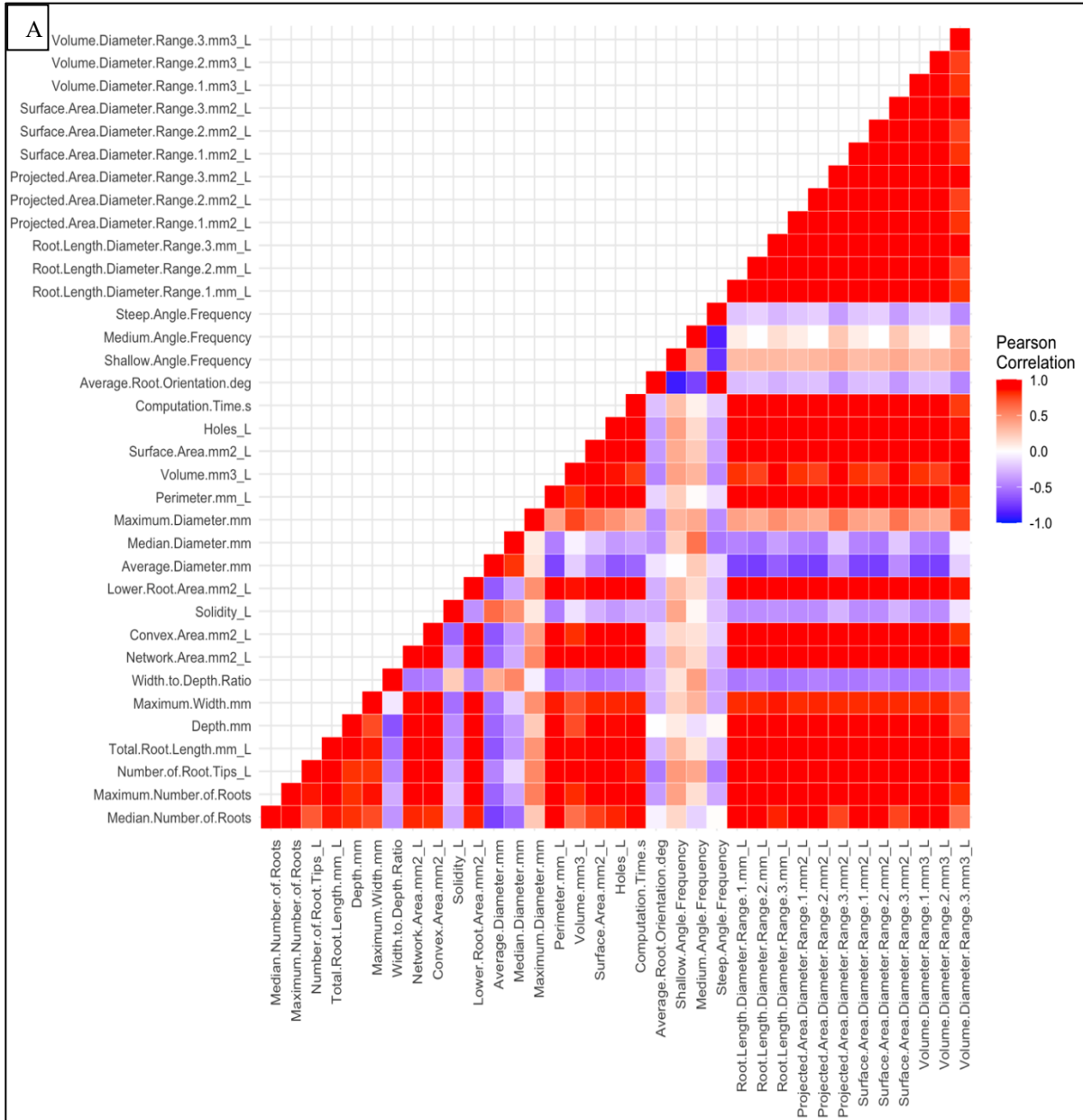
Figure 4. Correlation matrices of root traits of (A) *V. rupestris* and (B) *V. riparia*.
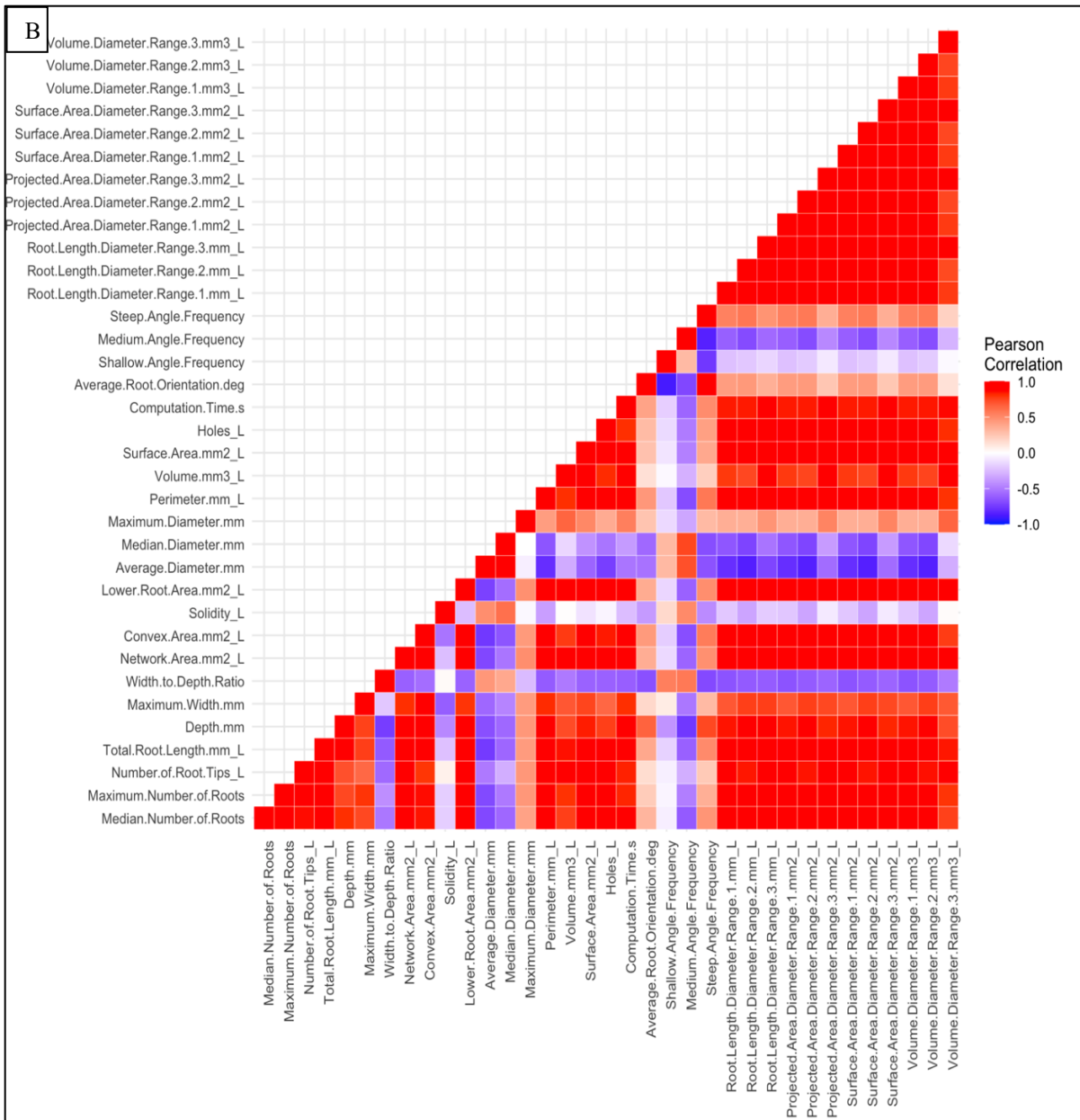
Figure 4. continued
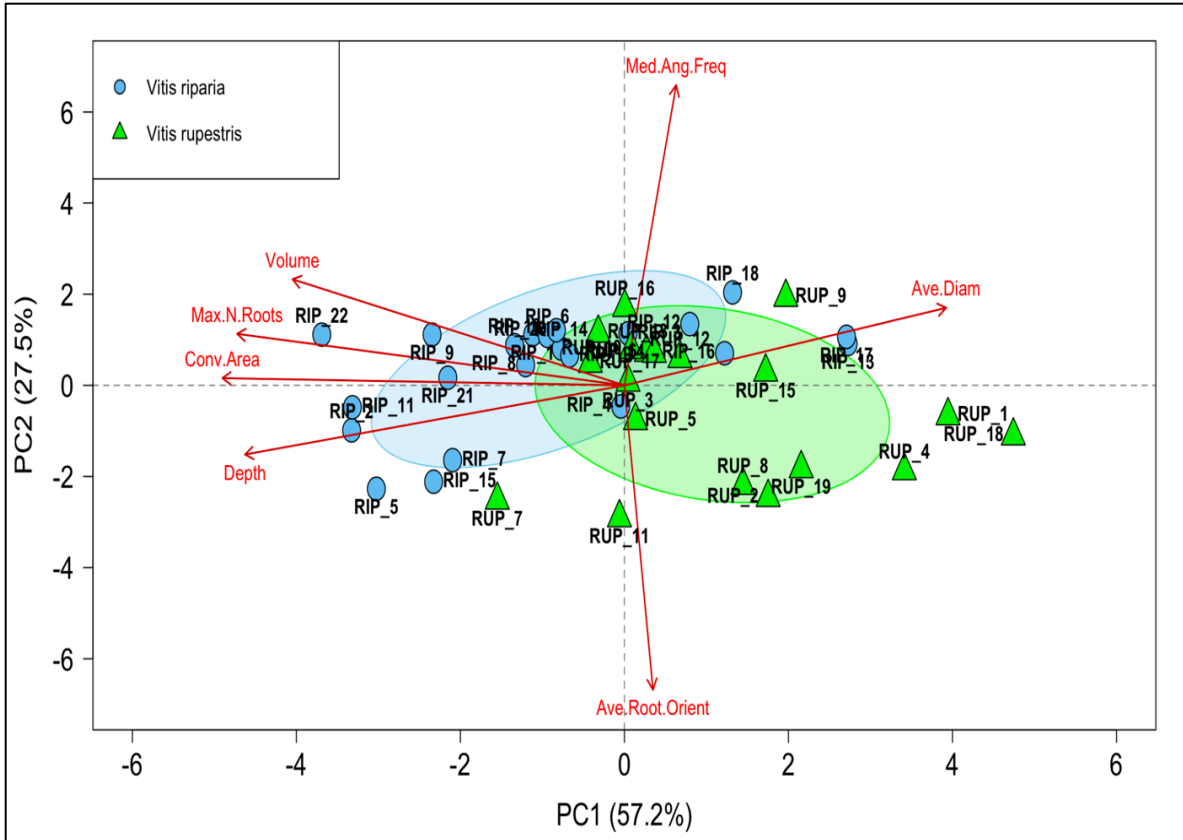
Figure 5. PCA plot for seven uncorrelated traits in *V. rupestris* and *V. riparia*. Each data point represents a *V. riparia* (blue circle) and a *V. rupestris* (green triangle) accession included in the analysis. The direction of arrows indicates the correlation and contribution of traits to the first two components, which represent 57.2% and 27.5% of the variation, respectively. The ellipses illustrate 95% confidence limits around the individuals in PC1 and PC2.

CHAPTER 2: IDENTIFICATION OF QUANTITATIVE TRAIT LOCI INFLUENCING ROOT SYSTEM ARCHITECTURE IN GRAPEVINE (*VITIS* SPECIES)

Introduction

The shape and distribution of grapevine roots are under both genetic and environmental control [1]. Previous results from the Kovacs Lab have shown that the impact of the environment is substantial even when the roots develop in uniform medium under the controlled greenhouse condition as the slight changes in temperature or other environmental components would affect the development of the plant [2]. Genetic factors, nonetheless, determine certain traits of root system architecture (RSA) in plants [3]. Quantitative trait locus (QTL) mapping is a powerful technology that uncovers natural alleles in plants which influence agronomically relevant quantitative traits. Identification of QTL has been the most common approach to understand the genetic underpinnings of RSA in several other plant species. For example, QTL for root length have been mapped in wheat [4-8], soybean [9-11], maize [12] and barley [13], for surface area in wheat [7], sorghum [14] and soybeans [10], for emergence angles in wheat [15], rice [16,17] and rapeseed [18], for lateral root and number of roots in soybean [11], for volume in wheat [7], for root system depth in barley [13], and for solidity in strawberry [19]. The potential of the mapping and deploying root trait QTL is demonstrated by QTL mapping and marker assisted selection of the *DRO1* gene from the deep-rooting highland rice cultivar Kinandang Patong [17]. The expression of the wild-type allele of *DRO1* in the root tip causes gravity-induced downward growth [20]. When this allele was introgressed into a shallow-rooting lowland rice cultivar, the maximum root length of the resulting plant increased more than two-fold, and it was able to maintain high yield performance under conditions of water-deficiency [20]. Another RSA-

related gene identified via QTL analysis is *ZmARGOS8* in maize. *ZmARGOS8* was implicated in the negative regulation of ethylene hormone response, and its overexpression results in reduced effect of ethylene on the lateral growth of maize roots [21].

RSA-influencing genes have been cloned as a result of both molecular studies and mutant analysis. The β-expansin gene, *GmEXPB2*, has been cloned from the differential screening of a soybean cDNA library. Overexpression of this gene is associated with elongation of hairy roots and efficient phosphate uptake in low phosphate level situation in soybean. Additionally, *GmEXPB2* expression leads to RSA responses to other abiotic stresses such as iron and water deficiency [22]. The maize *ZmPIN1a* gene has been cloned as a result of mutant analysis. *ZmPIN1a* is involved in auxin regulation, and its overexpression increase the number of lateral roots and prohibit their elongation [23].

The genetic basis of RSA is poorly understood in grapevine, despite efforts to breed rootstock cultivars and their nearly ubiquitous use in viticulture. Discovering regions of the grape genome that influence various traits is warranted because engineering the architecture of root systems offers a way to develop rootstock cultivars that are more resilient to environmental stress. Quantitative trait loci for RSA traits offers new tools for rootstock breeders to achieve that goal. As climate change-induced stress has an increasingly large impact on the quality of the fruit and the wine, there is growing interest in utilizing rootstocks to alleviate abiotic stress [24, 25].

In this study, I aimed to identify QTL that contribute to the traits I measured in chapter 1 using F1 interspecific hybrid vine population from a cross between *V. rupestris* (seed parent) and *V. riparia* (pollen parent). It has been expected that certain traits would segregate among F1 progeny and have large enough heritability. To test this hypothesis, I assessed the environmental

and genetic variance for 23 root traits and performed QTL analysis on those that had sizeable genetic variance.

Methods

  Study Design, Root System Generation, and RSA Data Extraction. Dormant one year-old cuttings from a panel of 245 different genotypes of F1 progeny obtained from a cross-pollination between *Vitis rupestris* Scheele B38 (seed parent) and *Vitis riparia* Michx HP-1 (pollen parent) were collected from the Darr Agricultural Center, Springfield, Missouri in December 2021 and January 2022. The cuttings were stored at 4°C for 12 to 15 weeks in moist sawdust. For each genotype, 10 cuttings were collected, and 5 cuttings were used as replicates for rooting in the greenhouse, Temple Hall, Missouri State University during June and July of 2022. The cuttings were rehydrated and planted in perlite medium following the same procedure and controlled conditions as used for the *V. rupestris* and *V. riparia* comparative analysis described in Chapter 1 of this thesis. Likewise, only the genotypes with at least three rooted replicates were selected for photographing. Overall, 162 genotypes of F1 progeny were used for analysis. The photographing of root system was also carried out with monochromatic camera and processed through Pylon Camera Software Suite 7.2.0. A representative image was saved as "bmp" file format for root system analysis. The RSA analysis of the F1 progeny was performed by "RhizoVision Explorer" following the same method as it was performed in the Chapter 1, and the total data of 23 root traits were extracted and analyzed from each root image and were stored in CSV format.

  Statistical Analysis. First, I examined the normality of data distribution by considering the histogram for each trait and applying log-transformation to normalize distribution of data

with non-normal frequency distributions (Appendix A-1). Subsequently, I performed correlation analysis among RSA traits using Pearson's correlation test and a correlation heatmap was generated to examine how root traits related to one-another, followed by regression analysis to examine the effect size of a certain root traits that were expected to influence on some other root traits. To obtain the degree of variation in the entire root system, I performed a principal component analysis (PCA). First, I conducted a PCA with all root traits regardless of whether any of the traits is correlated with one-another (Appendix A-4), followed by removal of correlated traits. The remaining 7 uncorrelated traits that explained a great number of variations in the population was used to generate a second PCA. Furthermore, the effect size of the initial mass on the maximum width and depth, the two main determinant of root system size, was examined by considering the R^2 value through applying a regression analysis. All statistical analyses were performed using R scripts, which are shown in the Appendix B.

To assess the effect of the environment and parental alleles on the phenotypic variance of RSA, 12 canes of the seed parent were also rooted in the same greenhouse, and the phenotype data of the resulting root systems were extracted. As all 12 of these individuals had identical genome, the variance in their RSA phenotype resulted exclusively from environmental factors, such as differences in the compactness perlite medium, temperature, humidity, etc. ($V_{P \text{ (Female parent)}} = V_{E \text{ (Female parent)}}$). Phenotypic variance among the 162 different F1 genotypes, on the other hand, represents the sum of both environmental and genetic variance, due to each individual having different combination of alleles ($V_{P \text{ (F1 progeny)}} = V_E + V_G$). Using $V_{E \text{ (Female parent)}}$ as an approximate value of V_E due to greenhouse rooting conditions, V_G of the F_1 progeny can be calculated using the equation, $V_{G \text{ (F1 progeny)}} = V_{P \text{ (F1 progeny)}} - V_{E \text{ (Female parent)}}$ [26]. Using the resultant variance information, heritability (H^2) was also calculated for all the traits based on the

equation $H^2= V_G \backslash V_P$ [26]. The values for environmental variance, phenotypic variance, genetic variance, and heritability were calculated using MS Excel.

QTL Mapping of Root Traits. For the F1 progeny, I generated a PCA of root traits with high heritability, including maximum and median number of roots, network area, convex area, lower root area, median diameter, and perimeter. Using the score values of the PCA as "derived traits" to characterize RSA, I performed a QTL analysis. Then, I performed single QTL mapping for all root traits to further explore the significant loci influencing the RSA of grapevine using the genotype-by-sequencing (GBS) marker-based genetic linkage map of the F1 population. The linkage map, consisting of 1,462 and 1,351 female- and male parent-informative markers, respectively, was constructed by Bhattarai et al [27] to map genetic loci of various traits in *V. rupestris* and *V. riparia* based on single nucleotide polymorphism (SNP) markers identified through the GBS approach. QTL analysis was performed by applying the double pseudo-testcross strategy implemented with the software MapQTL 6.0. The LOD threshold was determined by 1000 permutation tests to declare a significant QTL according to LOD values corresponding to QTL peaks. QTL peaks that reached above the LOD threshold value at 95% confidence interval or greater were considered significant.

Results

Correlation Analysis and Effect Size Examination in the F1 Population. Pearson correlation coefficient (r) values were similar to those measured in the *V. rupestris* and *V. riparia* accessions in Chapter 1. All size-associated traits, including volume, surface area, root length as a whole and in three diameter ranges, holes, perimeter, lower root area, convex area, network area, depth, median and maximum number of roots, and maximum width, had high pairwise

correlations ($r > 0.7$). Similarly, average root orientation and the frequency of steep angles had high positive correlation ($r = 0.9$, $p = 2.2e-16$), and average root orientation was negatively correlated with frequency of shallow angles ($r = -0.9$, $p = 2.2e-16$). Similar to parents, the root orientation and angle frequencies were not correlated to any of the size-associated root traits, and maximum root diameter had no correlation with overall size of the root system (Figure 6).

The regression analysis for the effect of steep angle frequency on depth had comparable results as in *V. riparia* accessions (Chapter 1), because the F-test value was significant ($F = 29.67$, $R^2 = 0.15$, $DF = 160$). Additionally, the maximum diameter significantly affected the depth ($F = 7.57$, $R^2 = 0.04$, $DF = 160$). The frequency of steep angles was also indicated to considerably affect average root orientation ($F = 3,146$, $R^2 = 0.95$, $DF = 160$). Conversely, the shallow angle frequency had no significant effect on the maximum width ($F = 0.26$, $R^2 = 0.001$, $DF = 160$) (Figure 7). The multivariate model consisting of sum of effects of steep angle frequency and maximum diameter in addition to the interaction of these two traits on depth was significant ($F = 19.97$, $R^2 = 0.27$, $DF = 158$), which clearly demonstrated the effect of these two variables on the depth, despite the lack of correlation between depth and either of these two traits. Propagule mass had no effect on the size of the root system as the R^2 values were very close to zero (Figure 8).

Exploratory Data Analysis. The PCA for all root traits illustrated that the first two principal components (PCs) captured 84.9% of the variation, with PC1 and PC2 explaining 71% and 13.9% of the variation, respectively. PC1 correlated well with the volume, surface area, projected area, root length, maximum diameter, perimeter, convex area, lower root area, number of roots, holes, maximum width, network area, and the volume and surface area of entire root system, while PC2 correlated strongly with shallow angle frequency, medium angle frequency,

average root orientation, steep angle frequency, width-to–depth ratio, and solidity (Appendix A-4). The highly correlated traits in PC1 all pointed toward a similar direction that would support the results of the Pearson correlation test. Following the removal of interrelated root traits, the PCA plot represented the cumulative variation of 83.3% in the first two PCs, of which PC1 explained 57.4 % and PC2 explained 25.9% (Figure 9).

Root Trait Heritability between F1 Progeny and Seed Parent. Statistical analysis conducted in the RSA data demonstrated high heritability ($H^2 > 50\%$) for several root traits, such as median and maximum number of roots, network area, convex area, lower root area, median dimeter, and perimeter. Negative heritability values were found for traits such as maximum diameter, volume, holes, average root orientation, and frequency of angles (Table 3), indicating that these traits were under strong environmental influence. Consequently, I could not investigate the genetic basis of these traits. The total root length, depth, and maximum width were also shown to be affected by the genotype ($30\% < H^2 < 45\%$). The angles, holes, and average root orientation, on the other hand, are indicated to be highly influenced by environmental factors, rather than the genotype of the F1 progeny.

QTL Mapping. QTL analysis was performed using PC1 scores derived from a PCA of the seven high-heritability traits ($H^2 > 50\%$), identified above. QTL resulting from this analysis all mapped to chromosome 10. A significant locus was mapped to maternal marker S10_4125692 in the position of 21.1 cM at $p < 0.02$, explaining 13.7% of total phenotypic variance (Figure 10). In addition, several markers were mapped at $p < 0.05$; a paternal QTL to the marker S10_3959571 at the 20.01 cM position was identified that explained 12.4% of total phenotypic variance. Another paternal QTL was at markers S10_1923190, S10_1923183, S10_1876993, at the 8.9 cM position explaining 12.1% of total phenotypic variance. An additional QTL was identified at marker

S10_1151498 at the 10.7 cM position which explained 12.4% of total phenotypic variance; however, since the two parents were heterozygous and contained identical alleles at this locus, this position could not be assigned to either parent. A maternal QTL was identified to the markers S10_4750952 and S10_4750953, in the 26.1 cM position which explained 12.1% of total phenotypic variance.

Mapping of individual traits lead to the finding of several QTL ($p<0.05$) on chromosome 10, most of which overlapped with the significant QTL obtained by using PC1 scores. The maternal QTL at position of 21.1 cM was linked to a variety of root traits, including maximum number of roots, maximum width, depth, lower root area, perimeter, root length and volume in the medium diameter range, explaining 12.4% to 16% of total phenotypic variance (Figure 11). The QTL at the heterozygous marker S10_1151498 at 10.7 cM was also linked to several root traits including maximum width, network area, lower root area, and volume in medium diameter range, explaining 12.3% to 13.5% of total phenotypic variance. A maternal QTL was identified at markers S10_5004674, S10_5021135, S10_4750952, and S10_4750953, between positions of 26.1-29.5 cM. This QTL was linked to maximum width that explained 13.7% to 15.9% of total phenotypic variance. Another maternal QTL was identified at marker S10_3606765 at the 19.6 cM position; it was linked to maximum width and depth which explained 12.9% to 13.9% of total phenotypic variance. The paternal QTL at 20.01 cM also was linked to depth and maximum width and explained 13.4% to 14.6% of total phenotypic variance. Another paternal QTL near a telomere at 0 cM at marker S10_710185 was linked to maximum number of roots and explained 13.1% of total phenotypic variance. Furthermore, the paternal QTL in the position of 8.9 cM was linked to depth, explaining 12.6% of total phenotypic variance.

Discussion

Understanding the genetic basis of RSA of grapevine is vital for the viticulture industry, as identifying important gene markers can accelerate the breeding of rootstock varieties that are well-adapted to stressful environmental conditions.

Results of my QTL analysis were in agreement with heritability values, as significant QTL were identified for only those traits for which positive heritability values were measured. Traits with relatively high heritability values ($H^2 > 50\%$) were lower root area and perimeter, for which I identified at least one significant maternal QTL that influenced these traits. Network area also had high heritability, but a significant QTL linked to network area could not be assigned to either parent. Root length, maximum width, and depth also had measurable heritability, but at a lower level ($30\% < H^2 < 45\%$). QTL influencing all these traits were identified in mapping. On the other hand, QTL could not be identified to any of those traits for which heritability could not be detected. Traits such as maximum diameter, holes, average root orientation, frequencies of shallow, medium, and steep angles were negatively determined by genotype. These traits were likely to be under strong environmental influence. A previous MS student reported in his thesis research [2] comparable heritability values to the ones presented here for most of traits. He identified negative heritability for volume, average root orientation, frequencies of shallow, medium, and steep angles, and maximum diameter. Similar to my results, he found relatively high heritability for maximum number of roots, median diameter, and perimeter. In contrast, I found negative heritability for holes, while he found relatively high heritability for this trait [2]; the reason for this discrepancy is not known. The small R^2 value indicated slight variation of the maximum width and depth in response to initial mass which leads to the conclusion that the mass

of the propagules had no effect on the size of the root system in F1 progeny. The same conclusion has been reached in Chapter 1.

In this study, the amount of variation explained by the first two PCs, in either PCA for all root traits or PCA for seven uncorrelated root traits, were similar to the percent of variation explained in PCA approach for *V. rupestris* and *V. riparia*. Pearson correlation findings were also comparable to the correlation coefficient values obtained for *V. rupestris* and *V. riparia* accessions; the size-associated traits had the tendency to have positive pairwise correlations, and they were toward the same general direction in the PCA plot. Following QTL mapping for PC1 scores by considering seven root traits with high heritability as one phenotype, a maternal QTL was identified at marker S10_4125692 at *P*< 0.02. This marker was linked to a great number of size-related root traits when mapping for each of those traits individually. This led me to reach the conclusion that this maternal marker is an important locus that influences the overall root system of grapevine to a large degree. The QTL at marker S10_1151498 were also linked to PC1 scores at *P*<0.05 and several size-related traits; however, it could not be assigned to either parent because of its same heterozygous configuration in both parents.

The results of PC1 scores were surprising because I showed in the first chapter of this thesis that *V. riparia* accessions tend to develop larger root system than *V. rupestris* accessions. I expected, therefore, that most significant QTL influencing RSA traits would map to the *V. riparia* pollen parent of this population. My QTL data are in disagreement with this expectation. The likely reason is that pollen parent HP-1 is an atypical representative of the species *V. riparia.* HP-1, which was originally collected in South Dakota, develops into a small vine in Missouri. It grows into somewhat larger vines under the boreal climatic conditions of South Dakota and New York, but even in the northerly climate, its size is considerably smaller than the size of the seed

parent *V. rupestris* B38. QTL for root system width and depth were mapped to both the maternal and paternal genomes, indicating that alleles in *V. riparia* HP-1 also contribute to these size-related traits. For example, the maternal QTL at markers S10_4750953 and S10_4750952, in addition to paternal QTL at marker S10_3959571 were linked to maximum width and depth. Furthermore, the paternal QTL mapped to three markers at position 8.9 cM was linked to depth. Width and depth are the two most important determinant traits of the size of the root system representing vertical and horizontal growth, and the overall size of the root system.

To date, there has been no comprehensive analysis of the genetic underpinnings root system architecture in grapevine. Therefore, the results of this study may pave the way for a better understanding of how grapevine root features are determined genetically. As the sample size in this study was quite large, statistical analyses results are more reliable compared to those presented in Chapter 1. Both maximum diameter and steep angle frequency significantly influenced the depth of the root system which supported the widely accepted concept that sharp angles results in deeper root system. One limitation of this study was the lack of replicates of the pollen parent of the F1 population. This is because the pollen parent is plant of small stature and therefore produces insufficient shoot biomass. Because of this, heritability calculation and the explained variation for each trait of the root system was based on only the phenotype of the seed parent. Therefore, the negative and small heritability values for some root traits can not necessarily be influenced only by the environment; they might have been affected by genes in pollen parent that was missing in this study. Moreover, the environmental variance could not be accurately determined in this study since the planting of F1 genotypes was performed in greenhouse in which the control of environmental conditions had limitations. Also, it needs to be noted that the significant QTL that were mapped in this study cannot completely define the

genetic basis of RSA in grapevine. Although the sample size was large enough and included 162 different individuals, the QTL mapping needs to be repeated for at least one more growing season to be accepted as evidence. Our next QTL mapping project for the year 2023 will alleviate the uncertainty in our statistical analyses and will validate the conclusions regarding the identified QTL and the inheritance pattern.

References

1. Ollat N, Bordenave L, Tandonnet JP, Boursiquot JM, Marguerit E. Grapevine rootstocks: origins and perspectives. Acta Hortic. 2016;1136:11–22.

2. Thapa S. Analysis of root system architecture and QTL identification in grapevines [Master's Thesis]. Springfield, MO: Missouri State University; 2022.

3. Rogers ED, Benfey PN. Regulation of plant root system architecture: implications for crop advancement. Curr Opin Biotechnol. 2015;32:93–8.

4. Cane MA, Maccaferri M, Nazemi G, Salvi S, Francia R, Colalongo C, et al. Association mapping for root architectural traits in durum wheat seedlings as related to agronomic performance. Mol Breeding. 2014;34:1629–45.

5. Chen H, Wei J, Tian R, Zeng Z, Tang H, Liu Y, et al. A major quantitative trait locus for wheat total root length associated with precipitation distribution. Front Plant Sci. 2022;13:995183.

6. Liu J, Zhang Q, Meng D, Ren X, Li H, Su Z, et al. *QMrl-7B* enhances root system, biomass, nitrogen accumulation and yield in bread wheat. Plants J. 2021;10(4):764.

7. Iannucci A, Marone D, Russo MA, Vita PD, Miullo V, Ferragonio P, et al. Mapping QTL for root and shoot morphological traits in a durum Wheat×*t. dicoccum* segregating population at seedling stage. Int J Genom. 2017;2017:6876393.

8. Alemu A, Feyissa T, Maccaferri M, Sciara G, Tuberosa R, Ammar K, et al. Genome-wide association analysis unveils novel QTLs for seminal root system architecture traits in Ethiopian durum wheat. BMC Genom. 2021;22:1–16.

9. Chen H, Kumawat G, Yan Y, Fan B, Xu D. Mapping and validation of a major QTL for primary root length of soybean seedlings grown in hydroponic conditions. BMC Genom. 2021;22(1):132.

10. Prince SJ, Vuong TD, Wu X, Bai Y, Lu F, Kumpatla SP, et al. Mapping quantitative trait loci for soybean seedling shoot and root architecture traits in an inter-specific genetic population. Front Plant Sci. 2020;11:1284.

11. Manavalan LP, Guttikonda SK, Nguyen VT, Shannon JG, Nguyen HT. Evaluation of diverse soybean germplasm for root growth and architecture. Plant Soil. 2010;330:503-14.

12. Liu Z, Gao K, Shan S, Gu R, Wang Z, Craft EJ, et al. Comparative analysis of root traits and the associated QTLs for maize seedlings grown in paper roll, hydroponics and vermiculite culture system. Front Plant Sci. 2017;8:436.

13. Jia Z, Liu Y, Gruber BD, Neumann K, Kilian B, Graner A, et al. Genetic dissection of root system architectural traits in spring barley. Front Plant Sci. 2019;10:400.

14. Bernardino KC, Pastina MM, Menezes CB, Sousa SM, Maciel LS, Carvalho JG, et al. The genetic architecture of phosphorus efficiency in sorghum involves pleiotropic QTL for root morphology and grain yield under low phosphorus availability in the soil. BMC Plant Biol. 2019;19:87.

15. Alahmad S, El Hassouni K, Bassi FM, Dinglasan E, Youssef C, Quarry G, et al. A major root architecture QTL responding to water limitation in durum wheat. Front Plant Sci. 2019;10:436.

16. Vinarao R, Proud C, Zhang X, Snell P, Fukai S, Mitchell J. Stable and novel quantitative trait loci (QTL) confer narrow root cone angle in an aerobic rice (*Oryza Sativa* l.) production system. Rice. 2021;14(1):28.

17. Uga Y, Okuno K, Yano M. *DRO1,* a major QTL involved in deep rooting of rice under upland field conditions. J Exp Bot. 2011;62(8):2485-94.

18. Duan X, Wang X, Jin K, Wang W, Liu H, Liu L, et al. Genetic dissection of root angle of *Brassica napus* in response to low phosphorus. Front Plant Sci. 2021;12:697872.

19. Cockerton HM, Li B, Stavridou E, Johnson A, Karlström A, Armitage AD, et al. Genetic and phenotypic associations between root architecture, arbuscular mycorrhizal fungi colonisation and low phosphate tolerance in strawberry (*Fragaria × ananassa*). BMC Plant Biol. 2020;20:154.

20. Uga Y, Sugimoto K, Ogawa S, Rane J, Ishitani M, Hara N, et al. Control of root system architecture by DEEPER ROOTING 1 increases rice yield under drought conditions. Nat Genet. 2013;45:1097–102.

21. Wu B, Ren W, Zhao L, Li Q, Sun J, Chen F, et al. Genome-wide association study of root system architecture in maize. Genes. 2022;13(2):181.

22. Guo W, Zhao J, Li X, Qin L, Yan X, Liao H. A soybean β-expansin gene *GmEXPB2* intrinsically involved in root system architecture responses to abiotic stresses. Plant J. 2011;66:541-52.

23. Li Z, Zhang X, Zhao Y, Li Y, Zhang G, Peng Z, et al. Enhancing auxin accumulation in maize root tips improves root growth and dwarfs plant height. Plant Biotechnol J. 2018;16:86-99.

24. Arora NK. Impact of climate change on agriculture production and its sustainable solutions. Environ Sustain. 2019;2:95-6.

25. Warschefsky EJ, Klein LL, Frank MH, Chitwood DH, Londo JP, Wettberg EJBV, et al. Rootstocks: diversity, domestication, and impacts on shoot phenotypes. Trends Plant Sci. 2016;21(5):418-37.

26. Bayers D. Components of phenotypic variance. Nat Educ. 2008;1:161.

27. Bhattarai G, Fennell A, Londo JP, Coleman C, Kovacs LG. A novel grape downy mildew resistance locus from *Vitis rupestris*. Am J Enol Vitic. 2021;72:12-20.

Table 3. Traits measured in the female parent and the F_1 progeny. Mean, standard deviation (SD), variance in seed parent, variance in F_1, genetic variance (V_G) and heritability (H^2) calculated for 22 traits of the root system.

| Trait | Mean ± SD | | Phenotypic Variance (V_P) | | V_G | H^2 |
	♀ Parent	F_1	♀ Parent	F_1		
Median Number of Roots	3.66 ± 1.54	4.30 ± 2.27	2.38	5.18	2.79	0.53
Maximum Number of Roots	10.57 ± 3.19	13.23 ± 4.97	10.18	24.70	14.51	0.58
Number of Root Tips	93.41 ± 174.21	158.60 ± 163.48	30351.24	26725.82	-3625.42	-0.13
Total root length (mm)	853.32 ± 1015.21	1286.14 ± 1263.57	1030663.11	1596621.51	565958.39	0.35
Depth (mm)	92.66 ± 46.12	92.48 ± 55.15	2127.96	3041.89	913.93	0.30
Maximum width (mm)	51.66 ± 15.72	61.53 ± 21.13	247.27	446.74	199.46	0.44
Width-to-Depth Ratio	0.66 ± 0.29	0.84 ± 0.30	0.08	0.09	0.002	0.02
Network area(mm^2)	822.96 ± 562.69	1097.59 ± 918.10	316624.18	842922.91	526298.72	0.62
Convex area (mm^2)	3433.42 ± 2669.49	4453.73 ± 4100.21	7126181.91	16811763.60	9685581.69	0.57
Solidity	0.27 ± 0.08	0.30 ± 0.09	0.006	0.008	0.002	0.27
Lower root area (mm^2)	782.09 ± 575.77	1093.54 ± 897.59	331512.63	805684.48	474171.84	0.58
Average diameter (mm)	2.07 ± 0.46	2.08 ± 0.61	0.21	0.37	0.16	0.43
Median diameter (mm)	1.43 ± 0.19	1.38 ± 0.36	0.03	0.13	0.09	0.71
Maximum diameter(mm)	14.02 ± 3.45	14.07 ± 1.82	11.90	3.33	-8.57	-2.57

Table 3. continued

|						
Perimeter (mm)	1073.09 ± 907.79	1624.54 ± 1675.94	824098.45	2808789.19	1984690.73	0.70
Volume (mm^3)	5541.16 ± 5004.89	6952.85 ± 4522.69	25049009.5	20454779.35	-4594230.11	-0.22
Surface area (mm)	5113.16± 5262.38	6862.94 ± 5292.02	27692741.7	28005499.81	312758.07	0.01
Holes	129.83 ± 333.58	171.0 ± 209.07	111280.47	43711.71	-67568.76	-1.54
Average Root Orientation	55.78 ± 7.33	49.19± 4.25	53.84	18.14	-35.69	-1.96
Shallow Angle Frequency	0.19 ± 0.07	0.26 ± 0.04	0.005	0.002	-0.003	-1.34
Medium Angle Frequency	0.28 ± 0.07	0.33 ± 0.04	0.005	0.002	-0.002	-1.23
Steep Angle Frequency	0.52 ± 0.13	0.39 ± 0.07	0.01	0.006	-0.01	-1.67
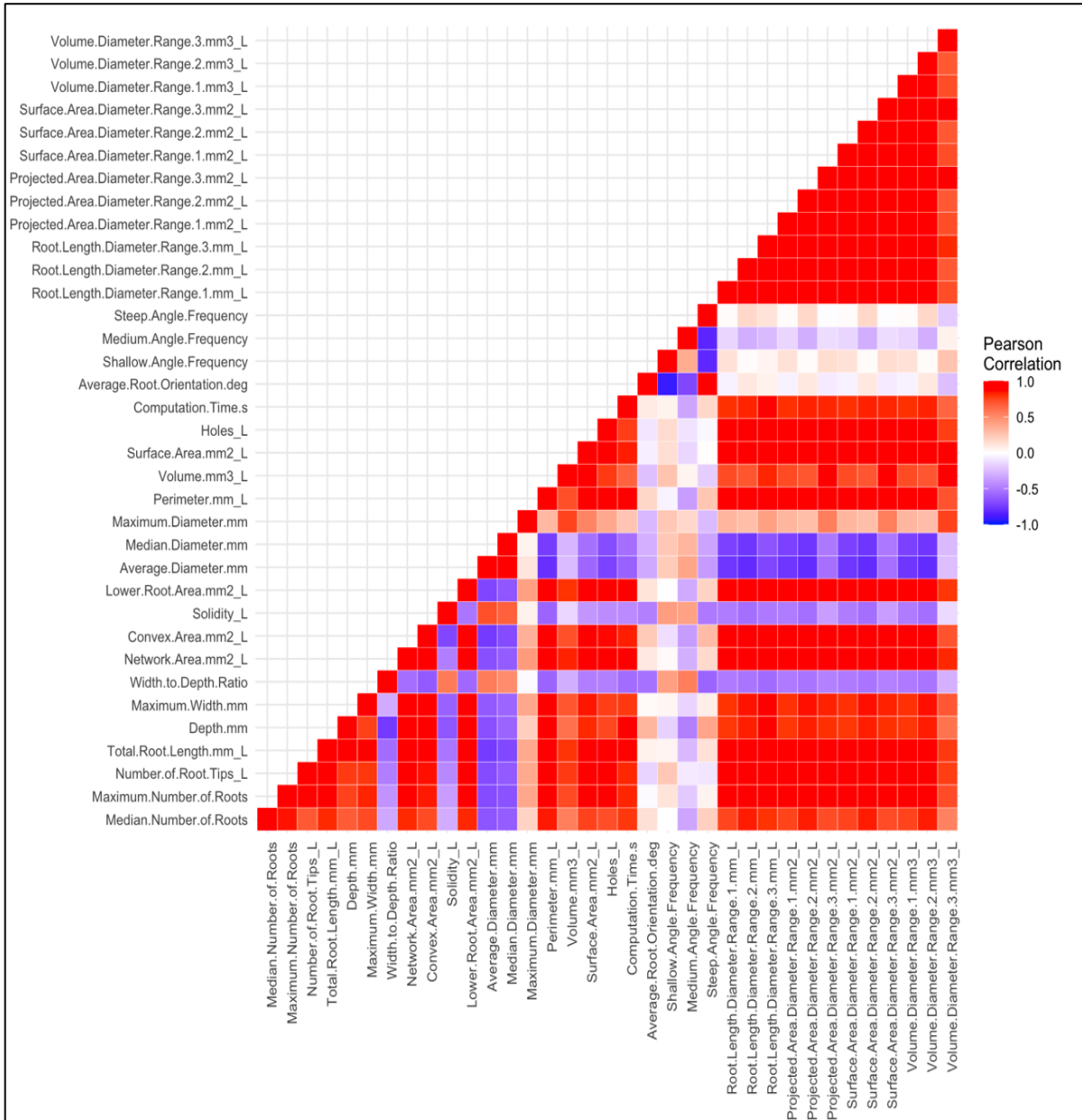
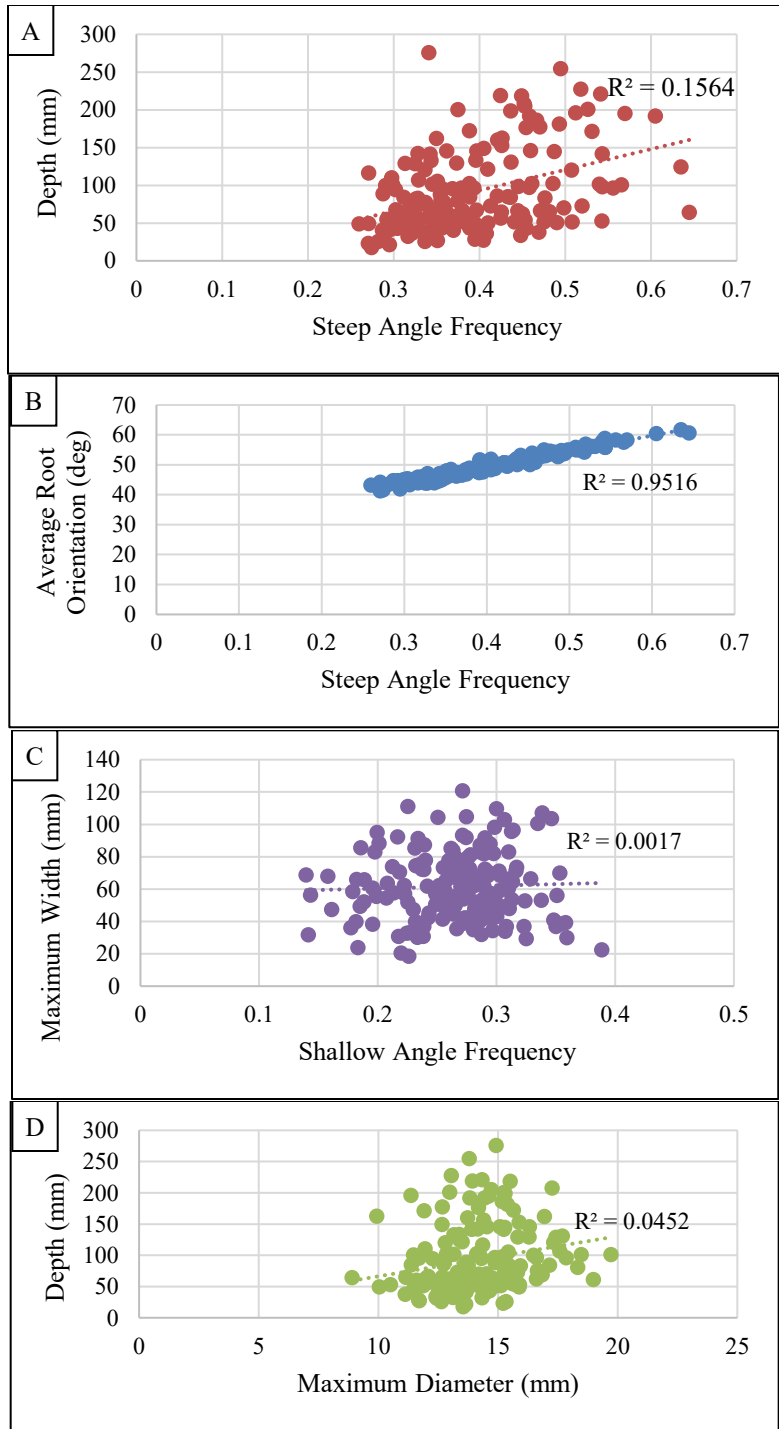Figure 6. Correlation matrix for root traits of F1 hybrid interspecific progeny

Figure 7. Regression analyses for the effect size of (A) the frequency of steep angles on depth, (B) frequency of steep angles on average root orientation, (C) frequency of shallow angles on maximum width, and (D) maximum diameter on depth. The R-squared values are shown.
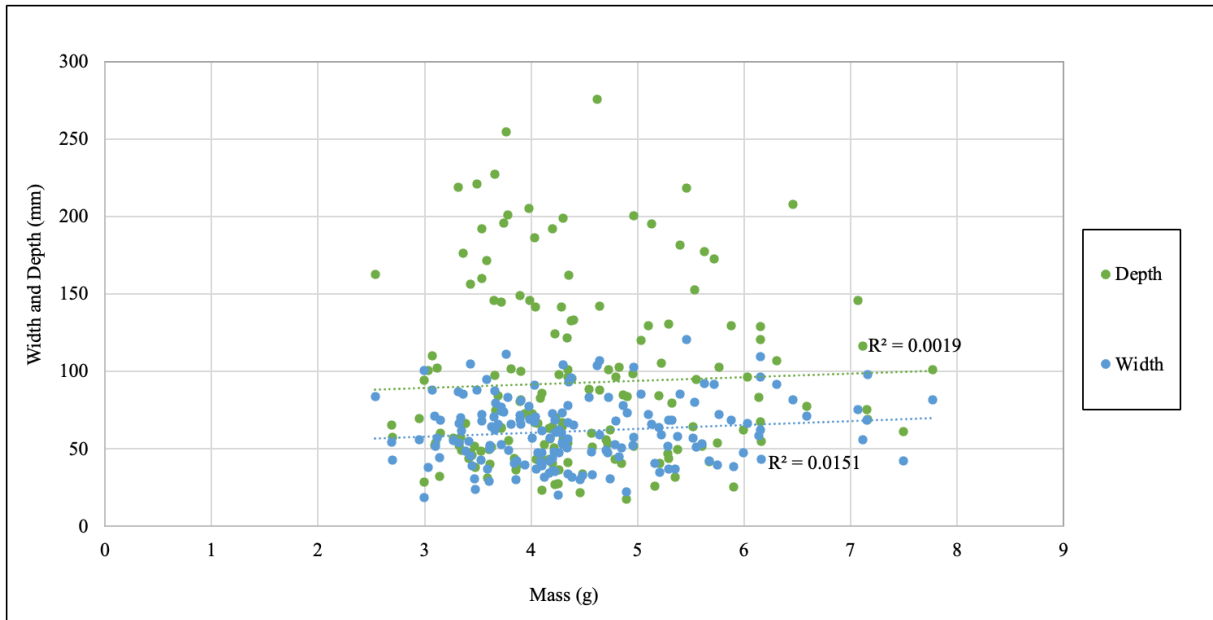
Figure 8. Regression analysis for the effect size of mass of the propagule on maximum width and depth in the F1 progeny. The R-squared values are shown.
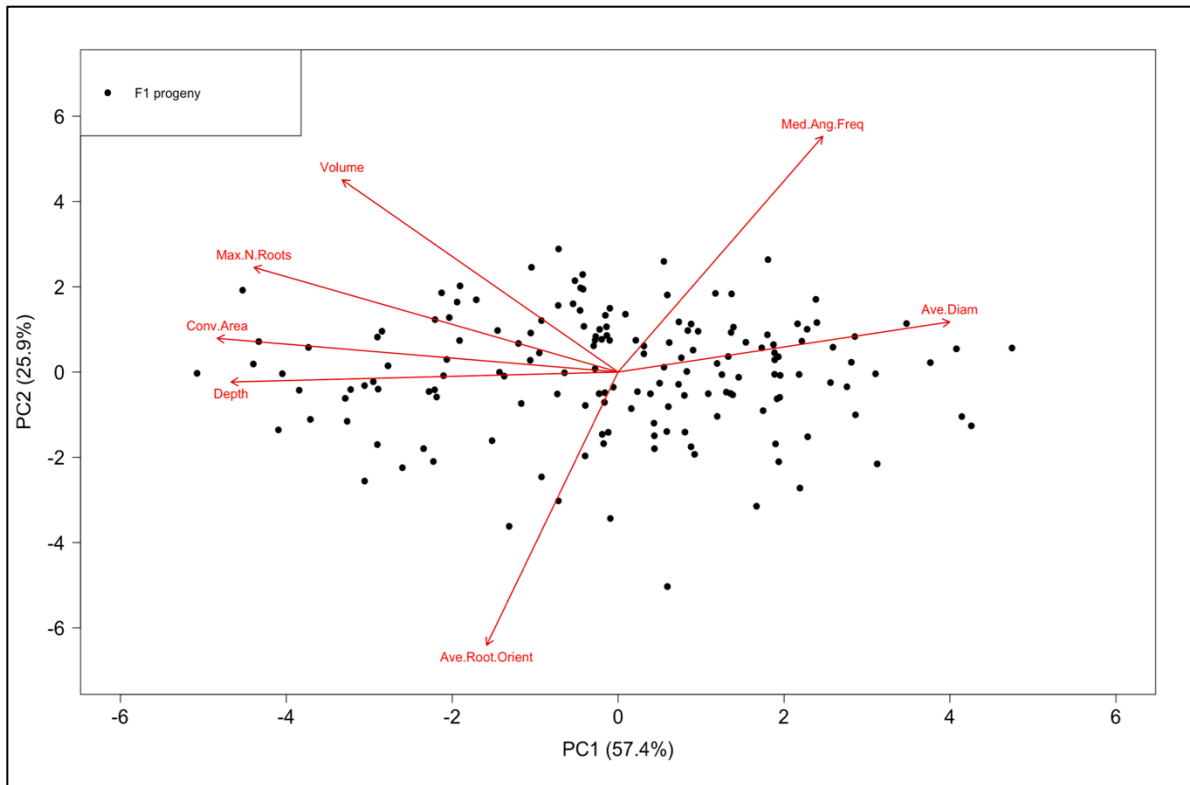
Figure 9. PCA plot for seven uncorrelated root traits. Each data point represents an F1 individual. The direction of arrows indicates the correlation and contribution of traits in individuals of the F1 population. PC1 and PC2 represent 57.4% and 25.9% of the variation, respectively.
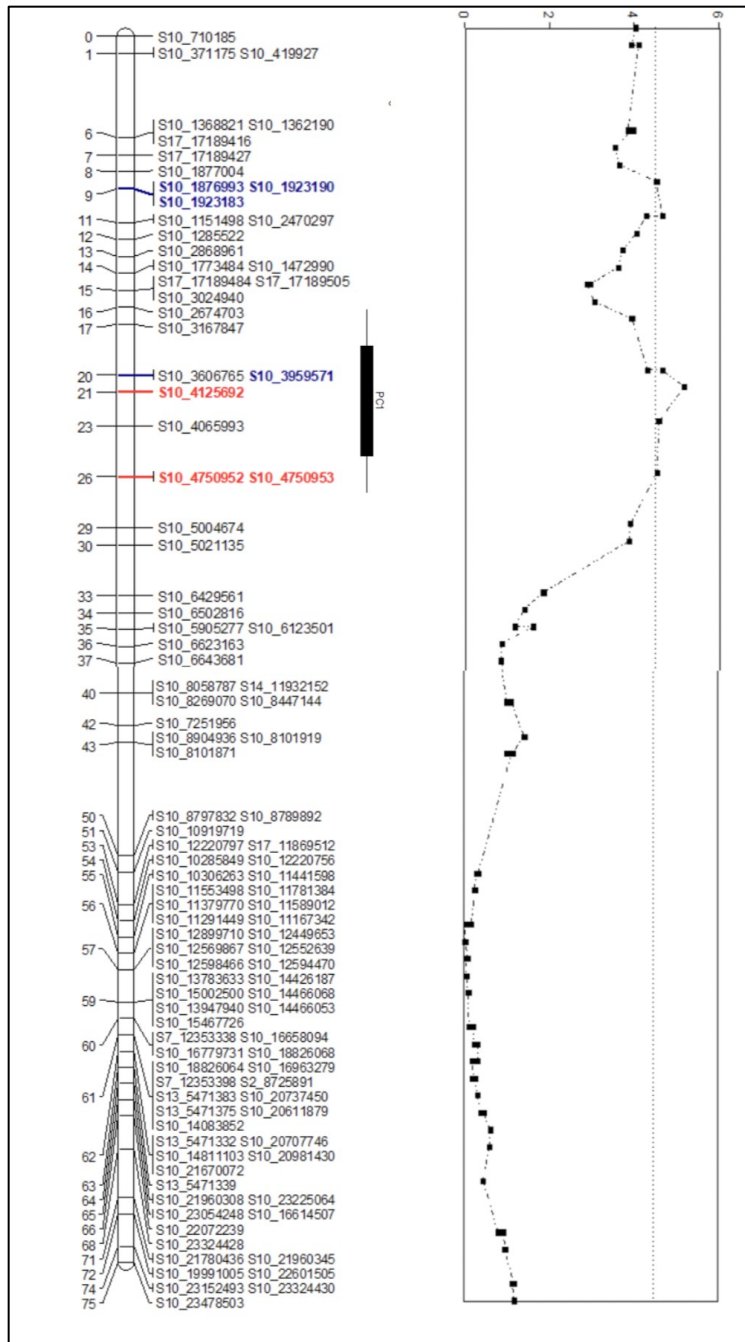
Figure 10. QTL for PC1 scores calculated for seven root traits with high heritability values. The QTL at marker S10_4125692 is at the same locus as the QTL for the number of roots, maximum width, depth, perimeter, lower root area, root length in medium diameter range in *V. rupestris* at *p*<0.02 (shown in red). QTL mapped to the same markers linked to maximum width and depth at *p*<0.05 are shown in bold. The maternal and paternal markers are indicated in red and blue, respectively.
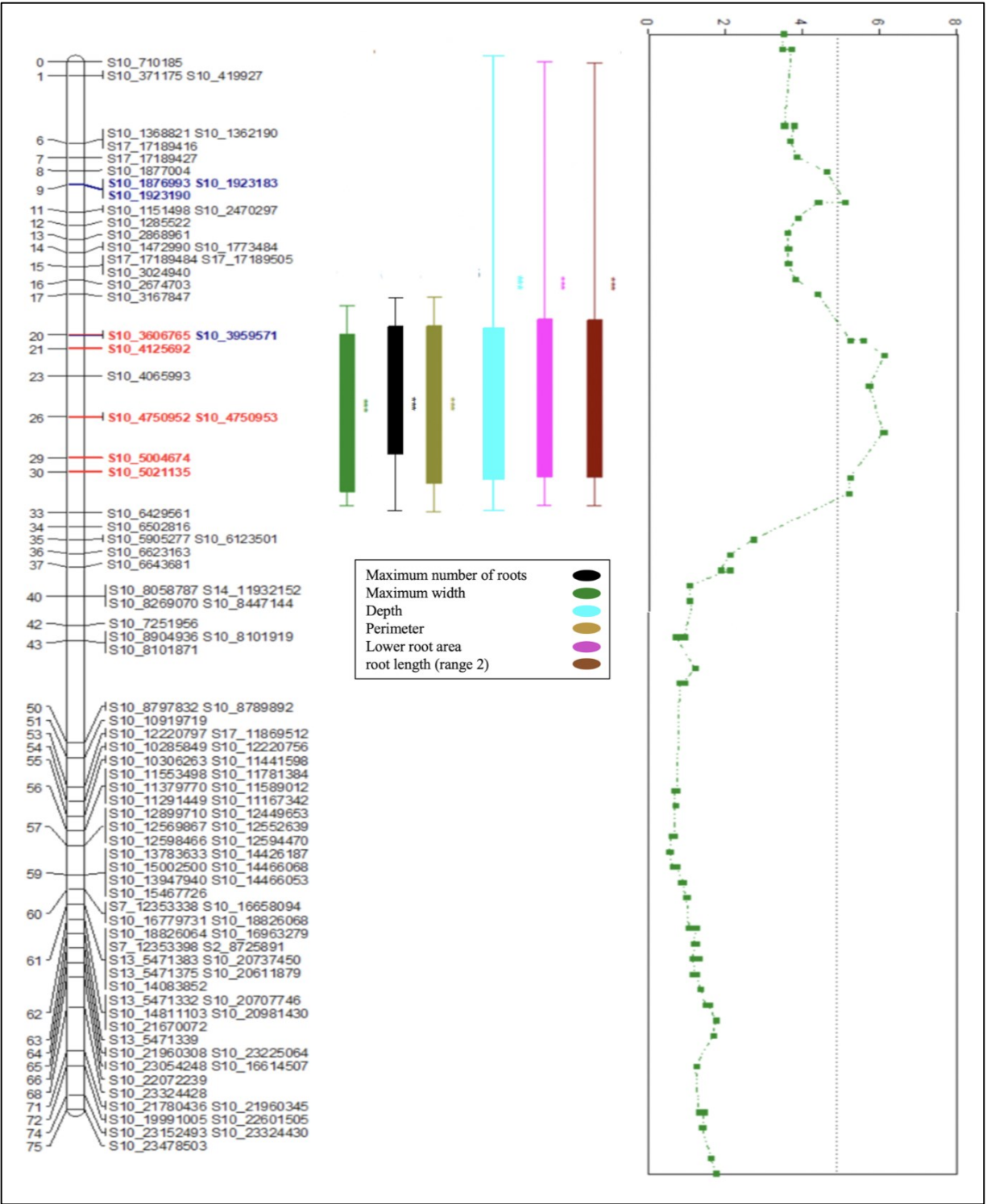
Figure 11. QTL mapped individually for seven root traits. The QTL peak shown on the LOD graph is for maximum width (*p*<0.05, LOD threshold= 4.9). The maternal and paternal markers are indicated in red and blue, respectively. The bars represent the confidence interval of all the traits that were mapped to the same locus as maximum width to the marker S10_4125692 (*p*<0.05).

SUMMARY

This thesis focuses on the root system of *V. rupestris* and *V. riparia*, two wild North American grapevine species which have been widely used as genetic resources in rootstock breeding for the viticulture industry [2]. The study examined the root system from two different perspectives: first, it addressed the question if the root system architecture (RSA) of these two species differed from one-another; second, it attempted to identify genomic loci in the gnome of a *V. rupestris* and a *V. riparia* accession that influenced RSA. I approached the first goal (Chapter 1) by generating and comparatively analyzing adventitious root systems from dormant cuttings of 22 *V. riparia* and 19 *V. rupestris* accessions. Principal component analysis (PCA) of seven uncorrelated root traits of the *V. riparia* and *V. rupestris* accessions showed that PC1 and PC2 collectively explained 84.7% of the phenotypic variation. The PCA plot indicated that the volume, maximum number of roots, convex area, and depth heavily loaded on PC1, and were directed toward the cluster of *V. riparia* accessions. These results confirmed the results of statistical comparisons which indicating that these traits had the tendency to be greater in *V. riparia* than in *V. rupestris.* These data were further substantiated by the results of binomial test.

My appraoch to the second goal (Chapter 2) was to map quantitaive triat loci (QTL) that contribute to RSA traits using an F1 progeny generated from a cross between *V. rupestris* (seed parent) and *V. riparia* (pollen parent). I peformed heritability calculation and identified traits that are under strong genetic control and those that are primarily determined by the environment. In my QTL analysis, I focused on the high-heritability traits, and I identified a maternal QTL, which influenced such traits as maximum width, depth, perimeter, lower root area, and the number of roots of the root system, explaining 12.4-16% of the total phenotypic variance. Using

PC-derived scores for 7 high-heritability traits as overall RSA phenotype, a QTL was identified which also mapped to an overlapping locus which explained 13.7% of the phenotypic variance. Interestingly, this mapping also identified several QTL that mapped to the paternal loci on chromosome 10, indicating that in this F1 progeny, both the seed and the pollen parent contribute to RSA and that chromosome 10 harbors genes that are key to determine RSA in grapevine. The data generated in this study provides grape breeders with valuable phenotype information and molecular markers for manipulating the size of the root system in new rootstock cultivars.

ADDITIONAL REFERENCES

1. Mudge K, Janick J, Scofield S, Goldschmidt EE. A history of grafting. Hortic Rev. 2009;3:437–93.

2. Riaz S, Pap D, Uretsky J, Laucou V, Boursiquot JM, Kocsis L, et al. Genetic diversity and parentage analysis of grape rootstocks. Theor Appl Genet. 2019;132:1847–60.

3. Klein LL, Miller AJ, Ciotir C, Hyma K, Uribe-Convers S, Londo J. High- throughput sequencing data clarify evolutionary relationships among North American *Vitis* species and improve identification in USDA *Vitis* germplasm collections. Am J Botany. 2018;105:215–26.

4. Liang Z, Duan S, Sheng J, Zhu S, Ni X, Shao J, et al. Whole-genome resequencing of 472 *Vitis* accessions for grapevine diversity and demographic history analyses. Nat Commun. 2019;10:1190.

5. Rogers ED, Benfey PN. Regulation of plant root system architecture: implications for crop advancement. Curr Opin Biotechnol. 2015;32:93–8.

6. Bhattarai G, Fennell A, Londo JP, Coleman C, Kovacs LG. A novel grape downy mildew resistance locus from *Vitis rupestris*. Am J Enol Vitic. 2021;72:12-20.
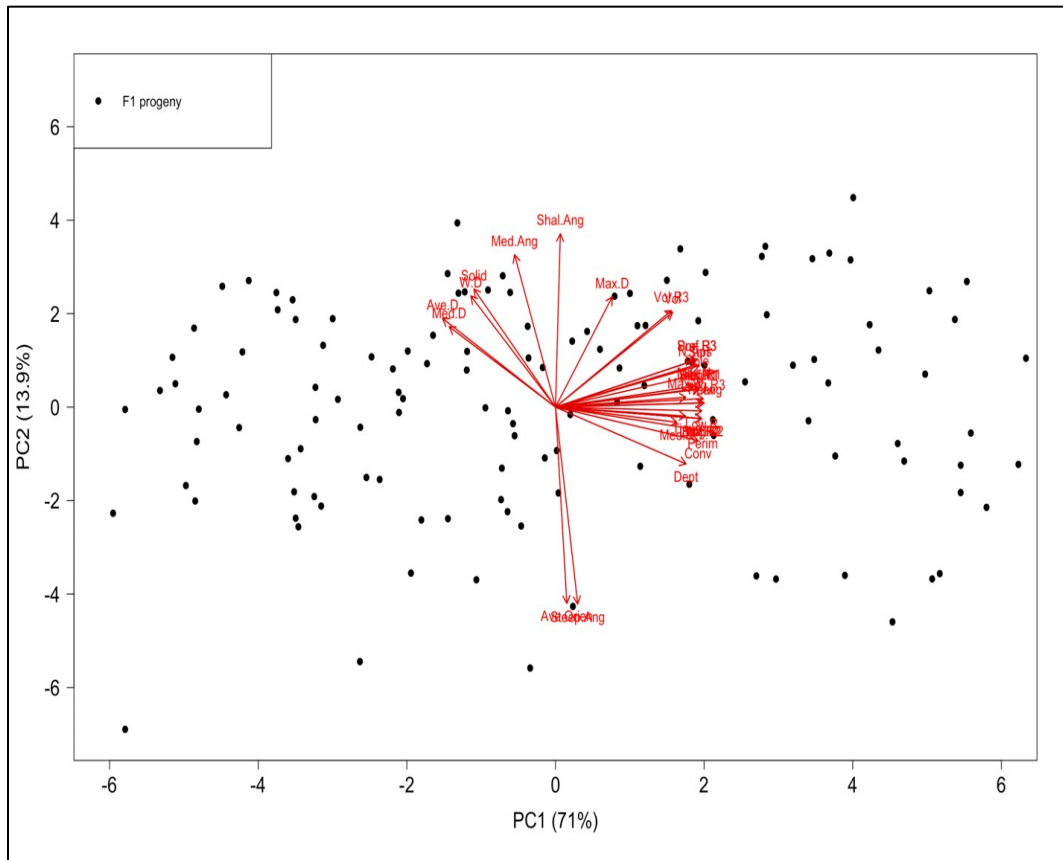
Appendix A. Supplemental Figures
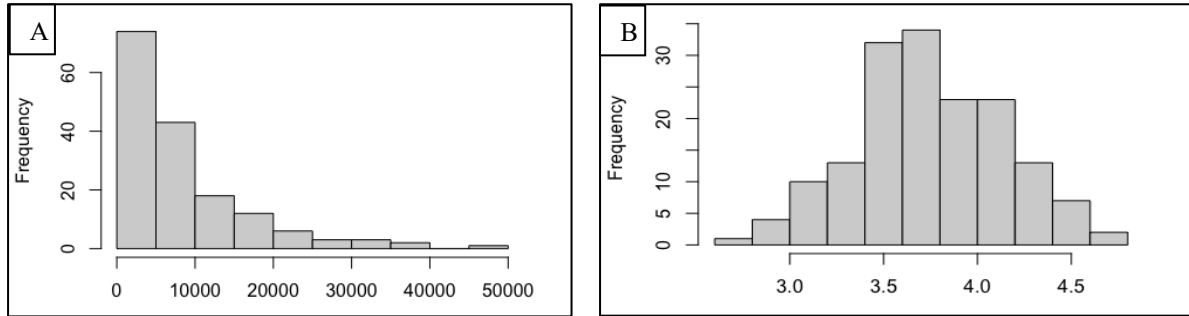
Appendix A-1. The histograms of frequency distribution of the total root length in the F1 progeny. Distribution of raw (A) and Log_{10}-transformed (B) root length data.
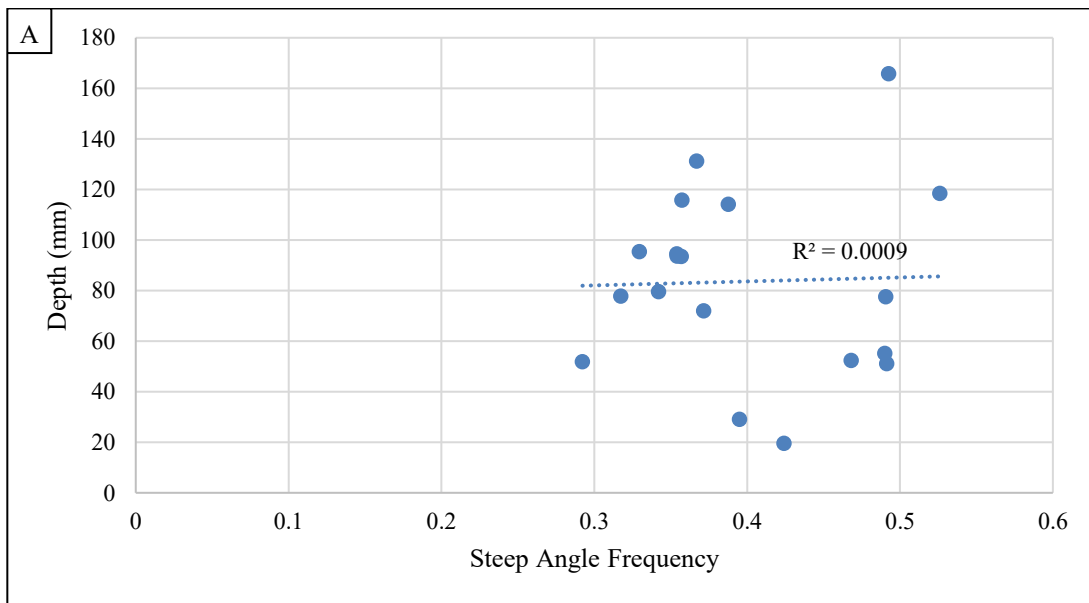
Appendix A-2. The scatter plots illustrating the effect of steep angle frequency on depth in *V. rupestris* (A) and *V. riparia* (B) ($p<0.05$).

Appendix A-2. continued

Appendix A-3. The PCA plot for all root traits in *V. rupestris* and *V. riparia*. The direction of arrows indicates the correlation and contribution of traits in the individuals of the two species. PC1 and PC2 represent 72.5% and 12.4% of the variation, respectively. The ellipses illustrate 95% confidence limits around the individuals in PC1 and PC2.

Appendix A-4. PCA plot for all root traits. Each data point represents an F1 individual. The direction of arrows indicates the correlation and contribution of traits in the individuals of F1 population. PC1 and PC2 represent 71% and 13.9% of the variation, respectively.

Appendix B. R Scripts

Appendix B-1. R script to generate correlation heatmap

```
Data.F1_35.traits <- read.csv("~/Desktop/Data analysis_Thesis_F1/Data F1_35 traits.csv",
header=TRUE)
options(max.print = 10000)
cor(Data.F1_35.traits [,2:36])
View(Data.F1_35.traits [,2:36])
install.packages("ggplot2")
library(ggplot2)
install.packages("reshape2")
library(reshape2)
cormat3 <- cor( Data.F1_35.traits[,2:36])
m.cormat3 <- melt(cormat3)
 head(m.cormat3)
get_lower_tri<-function(cormat3){
   cormat3[upper.tri(cormat3)] <- NA
```

```
    return(cormat3)
  }
  get_upper_tri <- function(cormat3){
    cormat3[lower.tri(cormat3)]<- NA
    return(cormat3)
  }
  upper_tri <- get_upper_tri(cormat3)
m.cormat3 <- melt(upper_tri, na.rm = TRUE)
ggplot(data = m.cormat3, aes(Var2, Var1, fill = value))+
 geom_tile(color = "white")+
 scale_fill_gradient2(low = "blue", high = "red", mid = "white",
  midpoint = 0, limit = c(-1,1), space = "Lab",
  name="Pearson\nCorrelation") +
 theme_minimal()+
theme(axis.text.x = element_text(angle = 45, vjust = 1,
   size = 12, hjust = 1))+
 coord_fixed()
```

Appendix B-2. R script for PCA of root traits in F1 progeny

```
PCA.F1.2022 <- prcomp (Data.F1_35.traits[,c(2:36)], scale. = TRUE)
summary(PCA.F1.2022)
s2<- summary(PCA.F1.2022)
install.packages("ellipse")
library(ellipse)
pch.group2 <- c(rep(21, times=162))
col.group2 <- c(rep("black", times=162))
tab2 <- matrix(c(PCA.F1.2022$x[,1], PCA.F1.2022$x[,2]), ncol=2)
c111 <- cor (tab2[1:162,])
l.x11 <- PCA.F1.2022$rotation[,1]*10
l.y11 <- PCA.F1.2022$rotation[,2]*10
l.pos11 <- l.y11
lo11 <- which(l.y11 < 0)
hi11 <- which(l.y11 > 0)
l.pos11 <- replace(l.pos11, lo11, "1")
l.pos11 <- replace(l.pos11, hi11, "3")
plot(PCA.F1.2022$x[,1], PCA.F1.2022$x[,2], xlab=paste("PC1 (", round(s2$importance[2]*100,
1), "%)", sep = ""), ylab=paste("PC2 (", round(s2$importance[5]*100, 1), "%)", sep = ""),
pch=pch.group2, col="black", bg=col.group2, cex=1, cex.axis=1.5, cex.lab=1.5, las=1, xlim =
c(-6, 6), ylim = c(-7, 7),
panel.last=arrows(x0=0, x1=l.x11, y0=0, y1=l.y11, col="red3", length=0.1, lwd=1.5))
text(PCA.F1.2022$x[,1], PCA.F1.2022$x[,2], labels=row.names(PCA.F1.2022$x),
pos=c(1,3,4,2), font=2)
text(l.x11, l.y11, labels=row.names(PCA.F1.2022$rotation), col="red", pos=l.pos11)
legend("topleft", legend=c("F1 progeny"), col="black", pt.bg=c("black"), pch=c(21), pt.cex=1)
```

Appendix B-3. R script functions used for PCA of root traits in parents

```
rownames(Parents.data.35.traits.names.abbr)<-Parents.data.35.traits.names.abbr[,1]
PCA.parents.2 <- prcomp (Parents.data.35.traits.names.abbr[,c(2:36)], scale. = TRUE)
summary(PCA.parents.2)
s<- summary(PCA.parents.2)
PCA.parents.2$sdev^2
pch.group <- c(rep(21, times=22), rep(24, times=19))
col.group <- c(rep("skyblue2", times=22), rep("green2", times=19))
tab <- matrix(c(PCA.parents.2$x[,1], PCA.parents.2$x[,2]), ncol=2)
tab1<- tab[1:22,]
tab2<- tab[23:41,]
ch1 <- chull(tab1)
ch2 <- chull(tab2)
install.packages("ellipse")
library(ellipse)
tab <- matrix(c(PCA.parents.2$x[,1], PCA.parents.2$x[,2]), ncol=2)
c1 <- cor (tab[1:22,])
c2 <- cor (tab[23:41,])
l.x <- PCA.parents.2$rotation[,1]*10
l.y <- PCA.parents.2$rotation[,2]*10
l.pos <- l.y
lo <- which(l.y < 0)
hi <- which(l.y > 0)
l.pos <- replace(l.pos, lo, "1")
l.pos <- replace(l.pos, hi, "3")
plot(PCA.parents.2$x[,1], PCA.parents.2$x[,2], xlab=paste("PC1 (",
round(s$importance[2]*100, 1), "%)", sep = ""), ylab=paste("PC2 (",
round(s$importance[5]*100, 1), "%)", sep = ""),
pch=pch.group, col="black", bg=col.group, cex=2.5, cex.axis=1.5, cex.lab=1.5, las=1, xlim = c(-
10, 14),ylim = c(-5,5),
panel.first= {
polygon(ellipse(c1*(max(abs(PCA.parents.2$rotation))*1), centre=colMeans(tab[1:22,]),
level=0.95), col=adjustcolor("skyblue2", alpha.f=0.25), border="skyblue")
polygon(ellipse(c2*(max(abs(PCA.parents.2$rotation))*1), centre=colMeans(tab[23:41,]),
level=0.95), col=adjustcolor("green2", alpha.f=0.25), border="green")
abline(v=0, lty=2, col="grey50")
abline(h=0, lty=2, col="grey50")},
panel.last=arrows(x0=0, x1=l.x, y0=0, y1=l.y, col="red3", length=0.1, lwd=1.5))
# Labels
text(PCA.parents.2$x[,1], PCA.parents.2$x[,2], labels=row.names(PCA.parents.2$x),
pos=c(1,3,4,2), font=2)
text(l.x, l.y, labels=row.names(PCA.parents.2$rotation), col="red", pos=l.pos)
legend("topleft", legend=c("Vitis riparia", "Vitis rupestris"), col="black", pt.bg=c("skyblue2",
"green2"), pch=c(21, 24), pt.cex=1.5)
```

Appendix C. Abbreviations

Max   Maximum
Min   Minimum
PC   Principal Component
PCA   Principal Component Analysis
QTL   Quantitative Trait Locus
RSA   Root System Architecture
SD   Standard Deviation
V_E Environmental Variance
V_G Genetic Variance
V_P Phenotypic Variance
AMF   Arbuscular Mycorrhizal Fungi
DF   Degrees of Freedom
SE   Standard Error